3-23-2018

Pulse Height Spectra Analysis of a Neutron Energy Tuning Assembly

Jason R. Stickney

Recommended Citation

Stickney, Jason R., "Pulse Height Spectra Analysis of a Neutron Energy Tuning Assembly" (2018). *Theses and Dissertations*. 1757.
https://scholar.afit.edu/etd/1757

PULSE HEIGHT SPECTRA ANALYSIS OF A NEUTRON ENERGY TUNING ASSEMBLY

THESIS

Jason R. Stickney, Captain, USAF

AFIT-ENP-MS-18-M-098

DEPARTMENT OF THE AIR FORCE
AIR UNIVERSITY

AIR FORCE INSTITUTE OF TECHNOLOGY

Wright-Patterson Air Force Base, Ohio

AFIT-ENP-MS-18-M-098

PULSE HEIGHT SPECTRA ANALYSIS OF A NEUTRON ENERGY TUNING ASSEMBLY

THESIS

Presented to the Faculty

Department of Engineering Physics

Graduate School of Engineering and Management

Air Force Institute of Technology

Air University

Air Education and Training Command

In Partial Fulfillment of the Requirements for the

Degree of Master of Science in Nuclear Engineering

Jason R. Stickney

Captain, USAF

MARCH 2018

ii

AFIT-ENP-MS-18-M-098

PULSE HEIGHT SPECTRA ANALYSIS OF A NEUTRON ENERGY TUNING ASSEMBLY

Jason R. Stickney

Captain, USAF

Committee Membership:

Capt J. E. Bevins, PhD
Chair

Dr. J. W. McClory
Member

Dr. E. J. Cazalas
Member

iv

AFIT-ENP-MS-18-M

Abstract

Neutron spectrum shaping is a potentially unique way to create a neutron energy spectrum that could be used to generate synthetic debris for nuclear forensics purposes. An energy tuning assembly (ETA) was previously designed and built for the purpose of irradiating samples with a combination of a thermonuclear and a prompt fission neutron spectrum. Initial research was performed to characterize the performance of the ETA at the Lawrence Berkeley National Laboratory 88-Inch Cyclotron using 33 MeV deuteron breakup on tantalum as the neutron source. This research analyzes detector responses collected from three EJ-309 detectors used to characterize the ETA generated neutron field.   The data analyzed consists of EJ-309 scintillator responses taken as full waveform measurements both with and without the ETA. A signal processing chain was developed to reduce the full waveform data into a pulse height spectrum. The primary goal was to develop a processing chain that optimized pulse shape discrimination performance to improve the discrimination between neutrons and gammas to thereby enable characterization of particle type down to the software threshold. This spectrum was then compared with a similar data set previously analyzed using a different pulse shape discrimination algorithm. It was found that the processing chain developed allowed for greater flexibility in determining the PSD parameters, which allowed for a greater degree of particle discrimination at low pulse heights.

Acknowledgments

To my lovely supportive wife, thank you for your continued support and encouragement.

I would like to express my appreciation to my committee members for their guidance and support throughout the course of this research effort. I would, also, like to thank Lt Rodney Carmona, who was on loan to the Air Force Institute of Technology for the programming support in this endeavor. I would finally like to thank the Bethany Goldblum and the Bay Area Neutron Group at the University of California-Berkeley for allowing me to use data that was collected at that location and their repository of codes.

Jason R. Stickney

Table of Contents

List of Figures

List of Tables

PULSE HEIGHT SPECTRA ANALYSIS OF A NEUTRON ENERGY TUNING ASSEMBLY

I. Introduction

1.1 Motivation

The U.S. has not tested a nuclear weapon since the Comprehensive Nuclear Test-Ban Treaty (CTBT) in 1992. However, subsequent administrations and Congress have reaffirmed the importance of the U.S. nuclear arsenal. The goal of maintaining an effective arsenal has been accomplished through the Stockpile Stewardship Program (SSP) implemented under President Clinton in 1995 [1].

Under this program, annual assessments are made of the health and status of each weapon system in the U.S. arsenal using computer simulations, component level testing, subcritical experiments using radioactive materials and high explosives, nonnuclear experiments, and analysis of historical data from past nuclear tests [2]. This type of testing has enabled the U.S. to maintain the nuclear weapons arsenal with confidence that the systems will work without a full test for over 25 years [3].

There are limits to what the Stockpile Stewardship Program and associated advanced simulation and computing capabilities can address. To cover these assessment gaps, the Department of Defense and Department of Energy have developed and maintained several unique facilities shown in Table 1. These facilities and their associated tools are, unfortunately, often undervalued or underfunded [4]. This results in gaps in capabilities or the inability to properly assess and certify systems. The scope of this problem is displayed in Figure 1 for nuclear weapon effects.

Table 1. Nuclear Weapons Effects Simulator Capabilities [5]**.**

Nuclear Weapon Environment	Test Facilities	Comments
Prompt and modified neutron	Sandia Pulsed Reactor III (or equivalent)* Annular Core Research Reactor White Sands Missile Range Fast Burst Reactor (also combined gamma) Los Alamos Neutron Science Center, Ion Beam Laboratory, and Rotating Target Neutron Source	For nuclear warhead subsystem space simulations For nuclear warhead components For ground systems, satellites, and interceptors For component tests and model validation
Prompt cold X-rays (plasma radiation source)	Upgraded Saturn and/or Double Eagle National Ignition Facility and/or Z-Refurbished (ZR)	For space system components/optics For future re-entry vehicle/re-entry body (RV/RB) material and interceptors
Prompt warm/hot X-rays (Bremsstrahlung source)	Upgraded Saturn and/or Pithon Modular Bremsstrahlung Source	For medium-dose electronics and cables For hardness surveillance and low-dose boxes
Prompt gamma	High-Energy Radiation Megavolt Electron Source (HERMES) III Pulserad (1150 or 958)	High dose-rates for strategic systems Low dose-rates for satellites and interceptors
Electromagnetic pulse	White Sands Missile Range Horizontally Polarized Dipole (HPD) Facility (2nd generation) Naval Air Warfare Center HPD Facility, Vertically Polarized Bounded Wave	For Army systems For aircraft and missiles
Source region electromagnetic pulse	HERMES III	For Army vehicles and field command, control, and communication systems
Impulse	Light Initiated High Explosive (LIHE) at Sandia National Labs Flyer-plate (magnetic or LIHE)*	For RV/RB internal components/mounts For future RV/RB aeroshells
Blast and shock	Large Blast Thermal Simulator Sandia National Laboratory Thunder Range	For ground vehicles, structures, non-ideal air blast (NIAB) simulations For RV/RB systems
Disturbed atmospheric radio frequency/infrared/ visible	Communication Chanel Scintillation (Wide-band Channel Simulator) Optical background (Nuclear Optical Dynamic Display System)	For military satellite communications, interceptor in-flight communications, and seekers

*Not currently available.
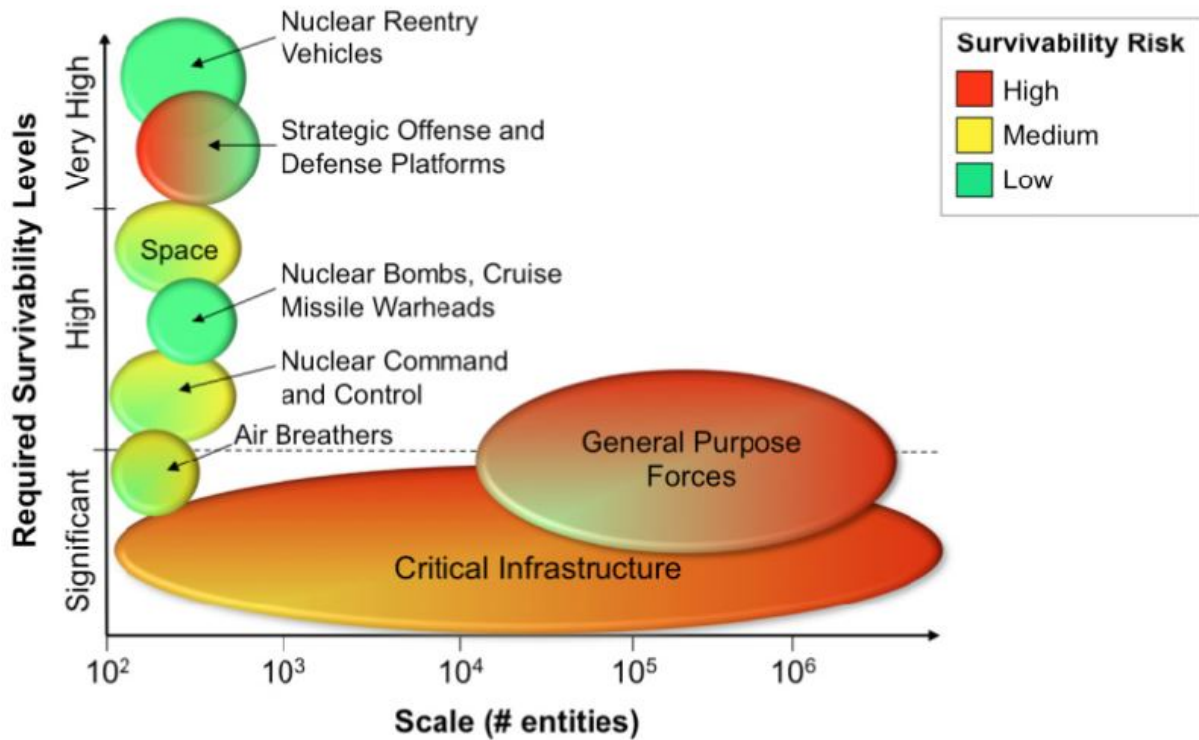
Figure 1. Current Survivability Risks of Critical Capabilities Against Nuclear Weapons [5]**.**

One of the more prevalent gaps is the ability to reproduce the neutron environment from a nuclear detonation, which includes neutrons from both the prompt fission neutron spectrum (from fission of fissile or fissionable material) and the thermonuclear spectrum (from D-T fusion). This gap extends to the production of post-detonation debris for the technical nuclear forensics attribution mission.

Generating the correct neutron spectrum is important for this mission because insufficient nuclear data exists for energy-dependent fission product yields [6]. The current Evaluated Nuclear Data File (ENDF) libraries are based on the original England and Rider evaluation with a literature cutoff date of 1989. The libraries also only contain the fission product yield for thermal, fast (fission - like spectrum with average energy of 0.5 MeV), and high (14.1 MeV) energy neutrons

3

[7]. There is very little data for neutron energies above 6 MeV, so the energy dependence when multi-energy fission is involved is difficult to benchmark [8]. There have been a number of mono-energetic measurements for select fission products and the uranium fission systems that could be used to supplement the ENDF libraries [9]–[12]. Even with these measurements, there is only a limited amount of data reported on select isotopes, thereby limiting the ability to generate synthetic debris with surrogate methods.

Several sources can match the spectral shape of the nuclear weapon neutron environment well in the keV to a few MeV range, but they lack in overall intensity. While some facilities are capable of producing the high energy thermonuclear component that is significant in causing displacement damage and electromagnetic effects, all have significant low energy components that would dominate nuclear reactions such as fission. There does not exist an operational facility which does all of the above. Additionally, even the few facilities shown in Table 1 that have been used to accomplish a portion of this mission space are at risk. Facilities like the Rotating Target Neutron Source (RTNS) or the Sandia Pulsed Reactor (SPR) have ceased operation [5], [13]. It is likely that the White Sands Missile Range (WSMR) Fast Burst Reactor (FBR) will be closing as soon as an alternative can be found [14].

With the possible exception of the National Ignition Facility (NIF), most other neutron sources were found to have a poor match to the proper timing profile and sufficient intensity. Getting these neutron spectral characteristics correct is important for studying radiation damage and understanding second order nuclear reactions. However, the neutron energy spectrum at NIF is a poor match for the desired environment. The NIF has a significant flux of neutrons due to D-T fusion that captures the thermonuclear portion of the thermonuclear and prompt fission neutron spectrum, but is has virtually zero prompt fission component.

To counter this, one approach would be to tailor the NIF neutron spectrum by using neutron moderators, filters, and reflectors to obtain the neutron spectrum required to replicate the weapon environment. Previous research developed an Energy Tuning Assembly (ETA) to form a generic thermonuclear and prompt fission neutron spectrum. The goal of the overall research effort is to reproduce the objective spectrum across an highly enriched uranium (HEU) foil located inside of the ETA at NIF [15]. Prior to fielding on NIF, an initial study was conducted to characterize the ETA performance at the Lawrence Berkeley 88-Inch Cyclotron.

For the experiment in question, the deuterons were accelerated to 33 MeV, and lined up for Cave 2, which is where the ETA and detectors were placed. Once in line with the room, the deuterons broke up on a tantalum target resulting in gammas and neutrons at approximately a 1:1 ratio [16]. The ultimate goal of this data analysis is to provide a development step for a planned NIF test that includes the generation of synthetic fission products. One of the short comings from the previous analysis was processing of only the pulse amplitude time data set, while very little of the collected data has been fully analyzed. This data includes several complete sets of foil activation, pulse height spectra (PHS), HEU activation, pulse-amplitude-time, and full waveform data [15].

1.2 Problem Description

This research analyzed data that was collected in a series of experiments in 2017 but very little of the full waveform data has been analyzed. The focus of this research includes developing an analysis chain for producing a neutron PHS and using the full waveform data to improve the particle type identification at low pulse heights. This data will then be compared to the results of the pulse amplitude time data previously analyzed.

1.2.1 Objectives

The objective of this research is to build an analysis chain for full waveform data from a validation experiment of the ETA at the 88-Inch Cyclotron at the Lawrence Berkeley National Labs. The hypothesis is that using the full waveform will allow for better pulse shape discrimination down to the software threshold thereby increasing the range of neutron energies which contribute to the pulse height spectrum. Specifically, this research aims to:

1. Determine optimal method and set of PSD parameters for each detector channel and data set

2. Determine the optimal signal analysis parameters for the integration window, threshold, and the pile-up rejection, baseline offset, and baseline smoothing algorithms

3. Generate a neutron pulse height spectrum (PHS) for each data set and detector channel

4. Compare the results to previous analysis using different analysis algorithms and methods

II. Background

2.1 Nuclear Reactions with Matter

This section explores the main neutron interactions in the context of spectral shaping and detection. Neutrons carry no charge and therefore cannot interact in matter by means of the Coulomb force. When a neutron interacts with a material, it is generally with the nucleus of the atom and thus is either absorbed or scattered [17]. The majority of neutron detectors utilize some type of conversion of the incident neutron into secondary charged particles. These particles can then be directly detected, and, with certain detectors, distinguished from other detected particle types.

2.1.1 Elastic Scattering

The microscopic cross section is higher for elastic scattering on smaller nuclei. In such an interaction, a fraction of the energy is transferred to the nuclei that was struck. The maximum energy loss for a neutron scattering off of a nucleus is given by

$$Q_{\max} = \left(1 - \frac{(A-1)^2}{(A+1)^2}\right) E \,,\tag{1}$$

where E is the initial neutron energy and A is the target atom mass. Equation 1 shows that low-A materials, such as hydrogen, require fewer scatters before the neutron's energy is brought down to thermal energies. However, the use high- and mid-A isotopes as the scattering medium allows more control over the neutron energy population from elastic scattering [15]. This process is important to the detectors, EJ-309s, used in this experiment. The EJ-309 uses a liquid organic scintillator based on the solvent xylene, chemical formula C_8H_{10}. Therefore, when a neutron hits a carbon nucleus, it is likely most of the energy will be retained from this exchange.

2.1.2 Inelastic Scattering

In inelastic neutron scattering, there is a difference in the total kinetic energy of the system before and after the interaction. The nucleus absorbs a portion of the incoming neutron's energy and is elevated to an excited state. The de-excitation of the nucleus after the inelastic neutron scattering usually results in the emission of a gamma ray as the nucleus reverts to its ground state. The general trend in the nuclear excited state structure is a decrease in the energy of the lowest lying nuclear state and an increase in the number of states with increasing Z. The increase in the number of states translates to a general increase in the inelastic scattering cross section for high Z materials, but these global trends are subject to significant local deviations because of shell and nuclear structure effects. The differentiation of the cross-section and variable energy loss can be exploited to tune the spectral shaping of the neutrons incident on the ETA in the 100s of keV to several MeV range [15].

2.1.3 (n, xn)

At high energies more than one neutron may be emitted after a reaction, resulting in reactions designated as (n, xn) reactions [18]. (n, xn) reactions are the result of the absorption of one neutron followed by the emission of two or more neutrons. This interaction is through the compound nucleus formation process or pre-compound emission of a neutron with lower energy. In the compound nucleus, the neutron shares its kinetic and binding energy with many nucleons thereby exciting the nucleus. The compound nucleus also "forgets" how it was formed, subsequently the decay of the excited compound nucleus results in a probability for one or more neutrons to "evaporate" [19]. The spectrum of neutrons evaporated at temperatures associated with fission differs from the temperatures associated with (n, xn) reactions for neutrons

with up to 14 MeV of kinetic energy. These differences in the emitted energy spectrum tend to be minor making the (n, xn) reaction highly beneficial to the function of the ETA [15].

2.1.4 (n, γ)

The final neutron reaction is the (n, γ) reaction, or more generally the (n, x) series of absorptive reactions. These reactions absorb a neutron to form a compound nucleus and emits a particle, such as a gamma, to de-excite. As absorbers, these reactions lower the overall neutron efficiency by removing neutrons from the system. The reduction in neutron economy is generally not beneficial in the nuclear forensics application where higher efficiencies and fission yields are desired.

However, the (n, γ) reactions can be useful in a few ways. First, the (n, x) reactions can be useful as an interaction mechanism for high energy neutrons. Second, the (n, γ) reactions are useful to absorb or "clean-up" any low energy neutrons resulting from over thermalization of the spectrum. Finally, (n, γ) reactions are useful as a diagnostic to measure the spectrum generated through activation analysis. For the EJ-309s used in this research, the effect is more an (n,α) reaction where the neutron is absorbed by a carbon nucleus, creating an unstable compound nucleus which alpha decays. This creates a third peak in the PSD spectrum which accounts for the alpha particles.

2.2 Neutron Spectroscopy

To characterize the ETA performance, the neutron energy spectrum must be measured. Efforts to perform neutron spectroscopy are limited by inelastic scattering that leads to a signal that is not necessarily proportional to the energy of the incident neutron. To overcome this limitation, many different techniques have been proposed, each with their own set of limitations.

The gold standard for neutron spectroscopy is the time-of-flight technique. This technique uses the time between the source generation, either measured from an accelerator beam or a chopper, and the time of detection to reconstruct the detected energy from the kinetic energy formula [20]. Time-of-flight methods can have very high measurement precision given the right combination of accelerator timing, flight path length, and fast detector response. In the ETA application, all of the initial timing is lost during the dozens to hundreds of interactions that occur within the ETA. Therefore, other techniques must be considered [15].

Proton recoil telescopes are another common neutron spectroscopy option. These telescopes use a thin hydrogenous material to scatter the neutrons into a detector located at a sufficient distance to subtend a small angle, thereby allowing reconstruction of the incident neutron energy from

$$E_p = E_n \cos(\theta),$$ (2)

where E_p is the detected energy of the recoiling proton, E_n is the incident neutron energy, and θ is the angle between the incident neutron beam and the detector. There is a tradeoff between energy resolution and efficiency, but proton recoil telescopes generally have extremely low detection efficiencies [17], [21]. Unfortunately, proton recoil telescopes will not work in the ETA application due to the lack of an incident collimated neutron beam.

A third option is capture-gated spectrometers. The idea is to record the total neutron energy through a series of multiple scatters within the detection volume, followed by capture with a highly absorbing dopant material such as ^{10}B. This approach has been successfully employed in many different configurations, and it would work for the 88-Inch Cyclotron neutron field measurements [17], [22], [23]. However, it could not be used in the ETA due to the needed detector being prohibitively large in order to obtain sufficient overall detection efficiencies for the high energy

10

neutrons. Additionally, since organic scintillators are typically used, the energy resolution is worse than the single scatter options due to the non-linearity of the response function.

The fourth and final option considered is neutron spectrum unfolding. This method has been employed with a variety of detection methods including Bonner spheres [24], gas proportional counters [17], activation foils [25]–[27], and liquid scintillators [28]–[30]. The foil activation method was chosen in this work for measuring the volume averaged thermonuclear and prompt fission neutron spectrum internal to the ETA. Liquid organic scintillators were chosen in this work due to their higher detection efficiencies and concurrent light yield measurements being conducted at the 88-Inch Cyclotron during the time of the collection.
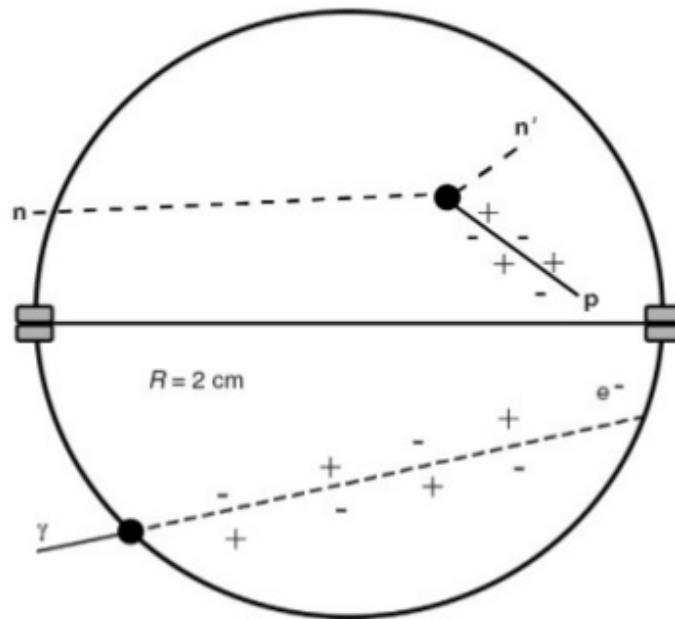
Figure 2. Example of particle interactions within a spherical proton recoil counter.

2.2.1 Liquid Scintillators

Scintillators are one of the oldest methods for radiation detection and as such have been studied extensively [17]. Organic scintillators work on the principle that incident radiation

11

populates excited states in the molecule. The states then depopulate via fluorescence. These emitted photons can be collected and converted to an electrical signal to allow for quantitative measurement of the energy deposited. For this experiment, liquid organic scintillators were used. These scintillators work via proton recoil as shown in Figure 2. Recoil detectors are more commonly used to detect fast neutrons because the cross sections for elastic scatter are substantial at high energies. Nuclear recoil detectors also make better spectrometers since they can better preserve energy information [17], [29].
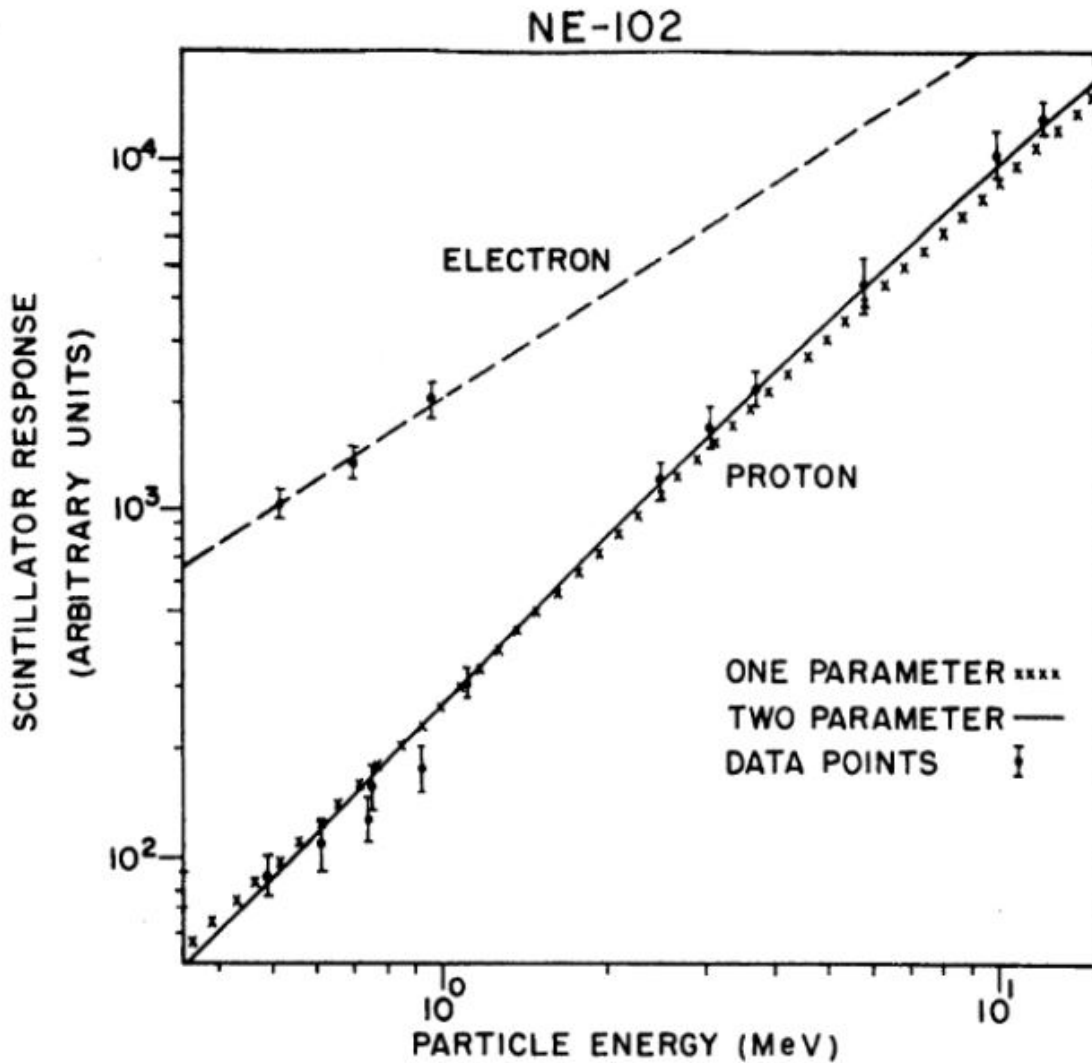
Figure 3. Comparison of the light yield from electron and proton energy deposition in NE-102 [17]**.**

12

The relation between the deposited energy and the light output of the scintillator varies by scintillator and is dependent on the particle depositing the energy, as shown in Figure 3. In Figure 3, electrons are the primary energy deposition mechanism for gamma interactions, while protons are the primary mechanism for neutron interactions within the scintillator. Accurately expressing the relationship between the energy deposition and light yield is crucial for unfolding the incident neutron flux [15], [17].

One drawback of liquid scintillators for the application of this experiment is their size. This limits their employment to outside of the ETA, which eliminates the ability to directly measure the thermonuclear and prompt fission neutron spectrum. However, they can measure the scattered neutron field around the ETA, thereby providing secondary and complementary experimental validation for the spectral shaping performance of the ETA [15].

Another drawback of liquid scintillators is their sensitivity to both neutron and gamma radiation. This can limit the ability to measure the neutron spectrum in a mixed field such as those present at NIF and the 88-Inch Cyclotron. A useful feature of some scintillators is the ability to use pulse shape discrimination to separate the neutron and gamma responses. The pulse shaped discrimination is described in Section 2.3.3 [15].

2.2.2 Neutron Spectrum Unfolding

Neutron spectrum unfolding solves the "inverse problem" to determine the unknown incident energy dependent neutron flux given a set of measurements and a known detector response function. There are several methods and techniques that have been developed over the years. These techniques can be divided into different classes depending on the algorithm used for the unfolding. The classes can be divided into the least-squares method, non-linear least-squares

method, and maximum entropy method. While all the methods are sufficient to unfolding, one of the primary differences between them is how they handle uncertainty [31].

All of these methods seek to solve the problem

$$S_i = \int R_i(\mathrm{E})\phi(E)dE , \qquad (3)$$

where S_i, is the is the measured value of the detector system for the ith iteration, $R_i(\mathrm{E})$ is the energy dependent response function for the ith measured channel, and $\phi(E)$ is the incident neutron energy spectrum. In the forward version of the problem, $R(E)$ and $\phi(E)$ are known and S has a unique solution. In the inverse problem, $\phi(E)$ is unknown, and Equation 3 has no unique solution due to the degeneracy created by representing a continuous function with a finite number of measurements [31].

Equation 3 can be approximated into a linear matrix, as shown in Equation 4. This approximation can be expanded into matrix form as shown in Equation 5 where M is the number of measurements and N is the number of neutron energy groups. Equation 4 also has no unique solution when N > M, and often not for N < M due to the correlations between the response functions [25], [31], [32].

$$\vec{S} = R\vec{\phi} \qquad (4)$$

$$\begin{pmatrix} S_1 \\ S_2 \\ \vdots \\ S_M \end{pmatrix} = \begin{pmatrix} R_{11} & R_{12} & \cdots & R_{1N} \\ R_{21} & R_{22} & \cdots & R_{2N} \\ \vdots & \vdots & \ddots & \vdots \\ R_{M1} & R_{M2} & \cdots & R_{MN} \end{pmatrix} \begin{pmatrix} \phi_1 \\ \phi_2 \\ \vdots \\ \phi_N \end{pmatrix} \qquad (5)$$

Equation 4 is often solved using iterative minimization approaches using the method of least squares instead of using the matrix form shown in Equation 5. This method is known as χ^2, which is given by

$$\frac{\chi^2}{n} = \frac{1}{n}\sum_i^M \frac{\left(\sum_j^N R_{ij}\phi_j^g - S_i\right)^2}{\sigma_i^2}.$$

(6)

In Equation 6, $n = (N-1)$, the number of the degrees of freedom, and σ_i is the uncertainty of the "ith" measurement [28], [31]. These methods are often modified to account for the non-negative flux requirements, smoothness of the solution, and the addition of a good starting spectrum to converge properly. If done properly, these modifications to the equation are useful in overcoming the degeneracy of the solution space to unfold spectra that are consistent with TOF measured spectra [15]. One limitation of the direct application of minimization or "goodness of fit" methods is the difficulty in assessing the uncertainty of the unfold [29], [31]. To overcome the difficulty in assessing the uncertainty of the unfold, maximum likelihood estimation and maximum entropy techniques were introduced [31], [33], [34]. These approaches construct a probability distribution over the degenerated solution space. This allows for the estimation of uncertainty.

Many computer programs have been developed to solve spectrum unfolding problems using variations of the basic mathematics described above [15], [35], [36]. Each code differs in the treatment of the uncertainty and the requirement for a guessed starting spectrum.

2.3 Signal Processing

2.3.1 Baseline Estimation

The baseline estimation step enables the extraction of the signal from the background noise. One important part of signal extraction is the correct identification of the baseline level of the data. Baseline estimating can be broken into three main types of algorithms. The first type of algorithms assumes the signal is all positive standing out from a zero-baseline level, then some kind of smoothing function would be an appropriate baseline. Alternatively, if the noise is assumed to fluctuate about a baseline level then some measure of center (median, mean, etc.) is more

15

appropriate. A third common type of analysis is continuous wavelet analysis, which does not have a separate baseline correction step as such; the baseline is automatically removed as part of the wavelet transformation [37]. This research used the second method because the algorithm uses a center moving average to dampen the noise, and baseline offset is determined to center the baseline at zero.

2.3.2 Pulse Pile-up and Pile-up Rejection

Pulse pile-up happens when pulses arrive within the pulse resolution time for the equipment. When a pulse pile-up event occurs, the system cannot measure the pulse heights correctly. In pulse pile-up, the system will simply record the two pulses as a single event with combined pulse amplitude, this is also known as peak pile-up shown in the bottom of Figure 4. If the pulses are spaced further apart, the system may simply accept both events separately and record them with incorrect pulse amplitude, this is known as tail pile-up shown in the top of Figure 4. In both cases the events will have the wrong recorded energy deposition and the pulse height and subsequent neutron spectrum will be incorrect [17], [35].
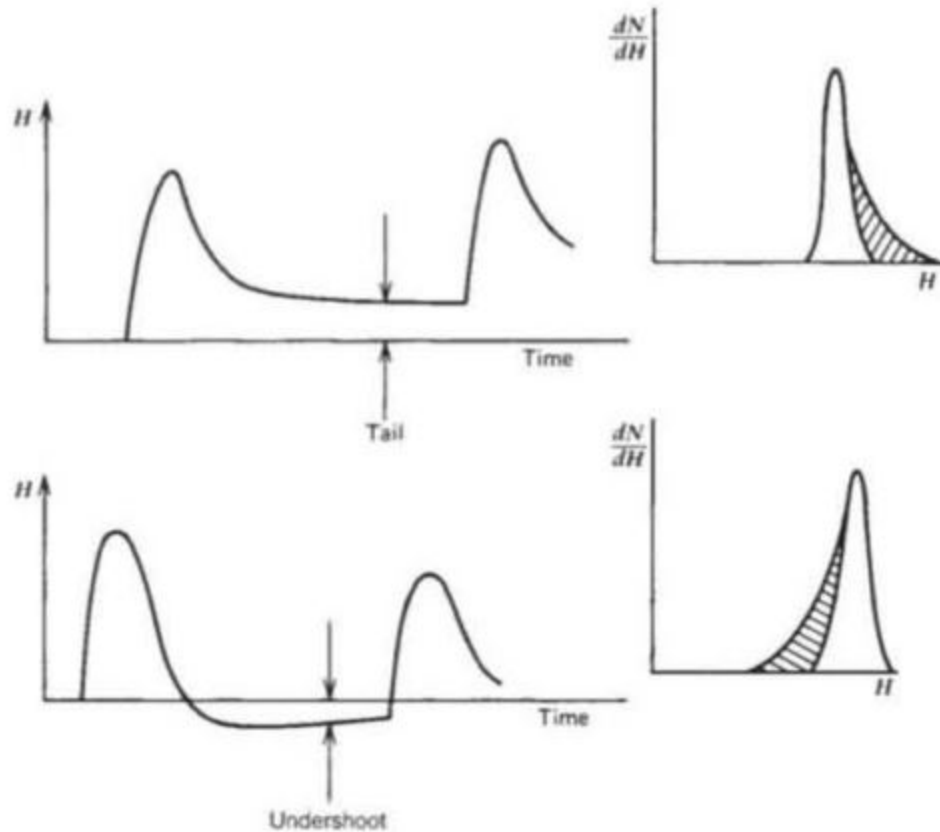
Figure 4. Pile-up from the undershoot of a preceding pulse and their effects on the pulse height spectrum [17]**.**

2.3.3 Pulse Shape Discrimination

Pulse shape discrimination (PSD) is the process of analyzing a pulse and discerning the particle type. In this research, the key distinction is whether the pulse came from a neutron or a gamma. This is necessary for the analysis of this data since the distribution of neutrons to total particles is approximately 50% as a result of the 33 MeV deuterons breakup on a Ta target, as [16]. As the detectors used to collect fast neutrons are sensitive to both fast neutrons and gammas, having a good PSD process is vital to discerning a spectrum of only neutrons.

There are two general approaches to carrying out PSD. The first is based on electronic methods of sensing the differences in the rise time of the pulse. The second derives the signal

based on the integral of the total charge over two different times [17]. The second is the method

used in this research for the analysis of the data. This method is possible due to the majority of

light emitted from scintillators employed having a characteristic decay time of a few nanoseconds,

with no longer lived component with a decay time of a few hundred nanoseconds. The fraction of

the delayed component is dependent on the type of incident radiation causing the initial excitation,

as shown in Figure 5 [17].
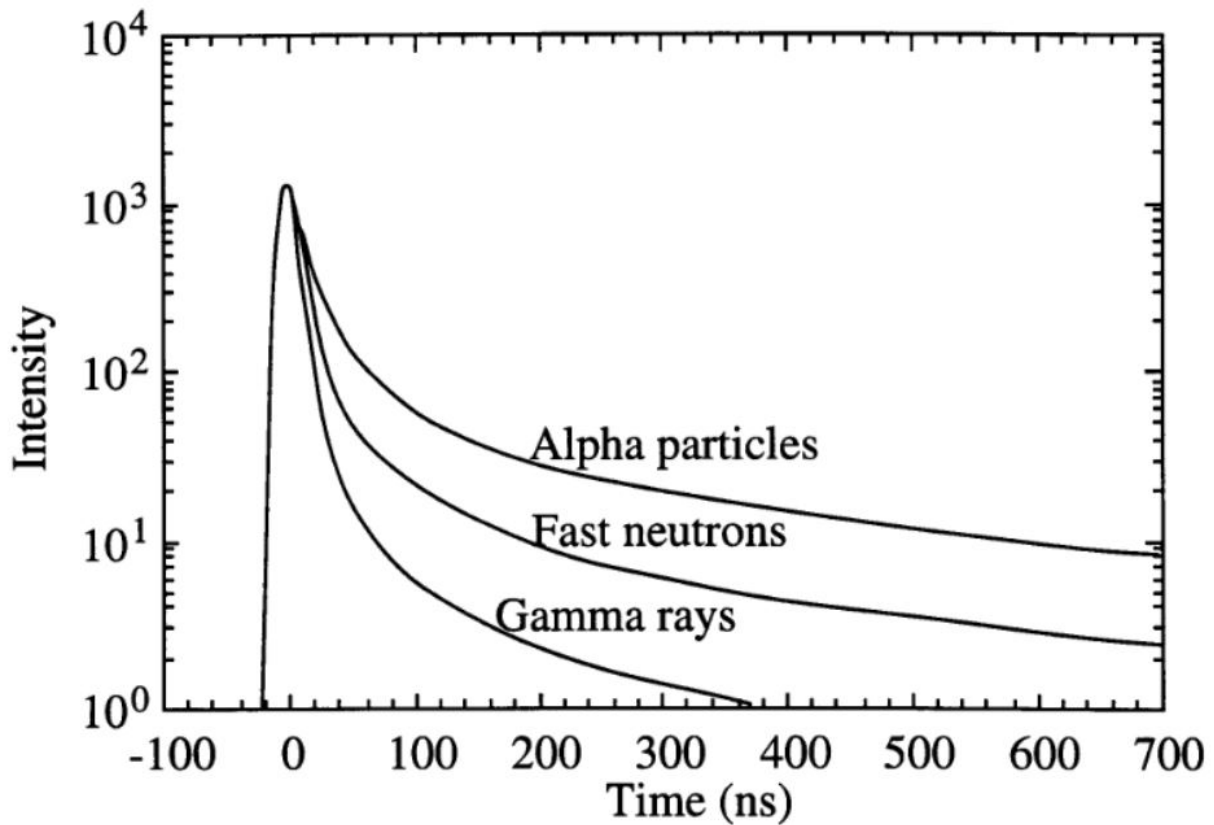
Figure 5. Comparison of the delayed light emission fraction as a function of the type of incident radiation for crystal scintillators [17]**.**

Two methods observed in this research were the Tail-to-Peak method, shown in Equation

7, and the Tail-to-Total method, shown in Equation 8, as a ratio of charge in tail of the pulse to the

total charge of the pulse [38].

$$PSD = \frac{\int_{tail_{start}}^{tail_{end}} Qdt}{\int_{peak_{start}}^{peak_{end}} Qdt} \qquad (7)$$

$$PSD = \frac{\int_{tail_{start}}^{tail_{end}} Qdt}{\int_{tot_{start}}^{tot_{end}} Qdt} \qquad (8)$$

Once a PSD method is chosen, a Figure of Merit (FOM) needs to be defined to quantify the PSD. In the case of this research the FOM chosen is shown in Equation 9

$$FOM = \frac{s}{\delta_{neutron} + \delta_{gamma}}, \qquad (9)$$

In Equation 9, s is the distance between the gamma and neutron peaks and δ is the full width at half maximum of the peaks in the PSD plot [39].

III. Methodology

The purpose of this thesis was to develop the method to process the raw pulse data and get a pulse height spectrum of the incident neutrons. The data was delivered in the ROOT format with each detector as a separate tree. These files were split into 1 GB sized files for data management purposes. Each tree contained full waveform pulses for all of the recorded events.

3.1 Experimental Setup

For this research, the experiment was conducted at the Lawrence Berkeley National Laboratory 88-Inch Cyclotron. A facility drawing is shown in Figure 6, and the setup of the three EJ-309 detectors in relation to the ETA is shown in Figure 7. The ETA and detectors were setup in Cave 02 in front of the 7-meter collimated flight path where the neutrons exited and interacted with the ETA and detectors. The detectors were positioned to collect the scattered neutron particles after interacting with the ETA. The data analyzed consists of EJ-309 scintillator responses taken as full waveform measurements both with and without the ETA. The EJ-309s used are 2" right circular cylinders filled with an organic scintillator composed of a xylene solution, $(CH_3)_2C_6H_4$.
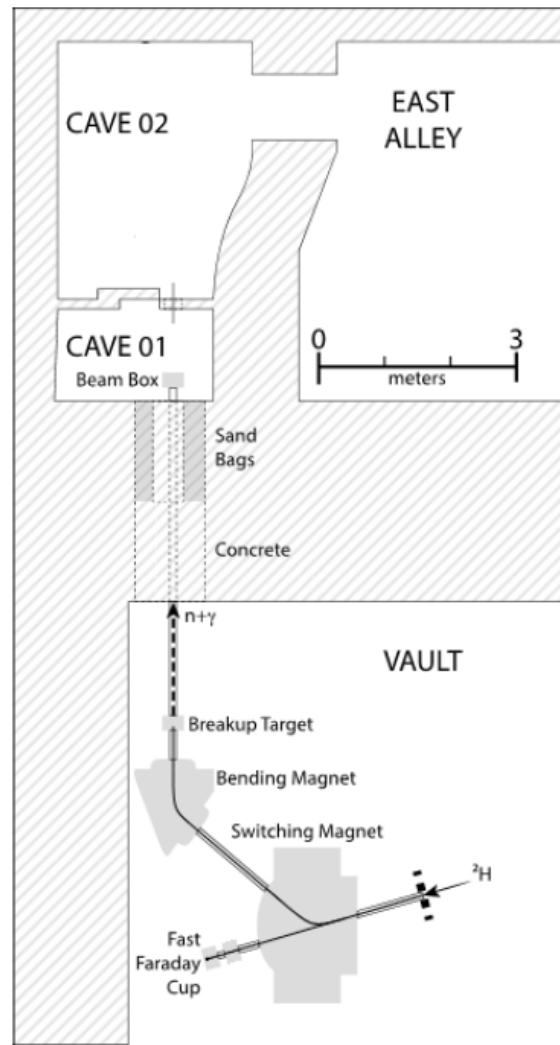
Figure 6. Schematic drawing of the Cyclotron and Cave 02, where the experiment was setup. The path of the deuterons, breakup into neutrons, and path of neutrons into Cave 02 is depicted.
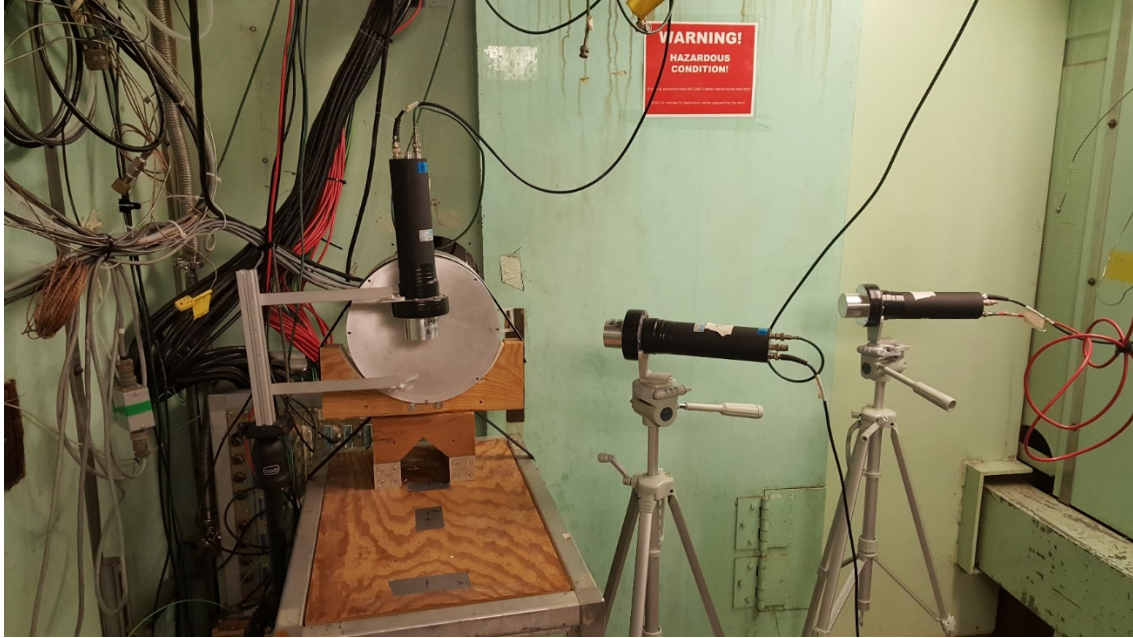
Figure 7. Experimental setup within Cave 02 at the 88-Inch Cyclotron. The ETA is the metal disk with detector 1 directly behind it. Detector 2 is centered 45° off axis from the ETA, and detector 3 is at 90°.

For each of the three detectors, calibration data was collected using an AmBe source, a ^{137}Cs source, and a ^{60}Co source. For this setup, the sources were taped to the side of the detectors for run 2 and the detectors were arranged equidistant from the source in run 3 as shown in Figure 8 and Figure 9.
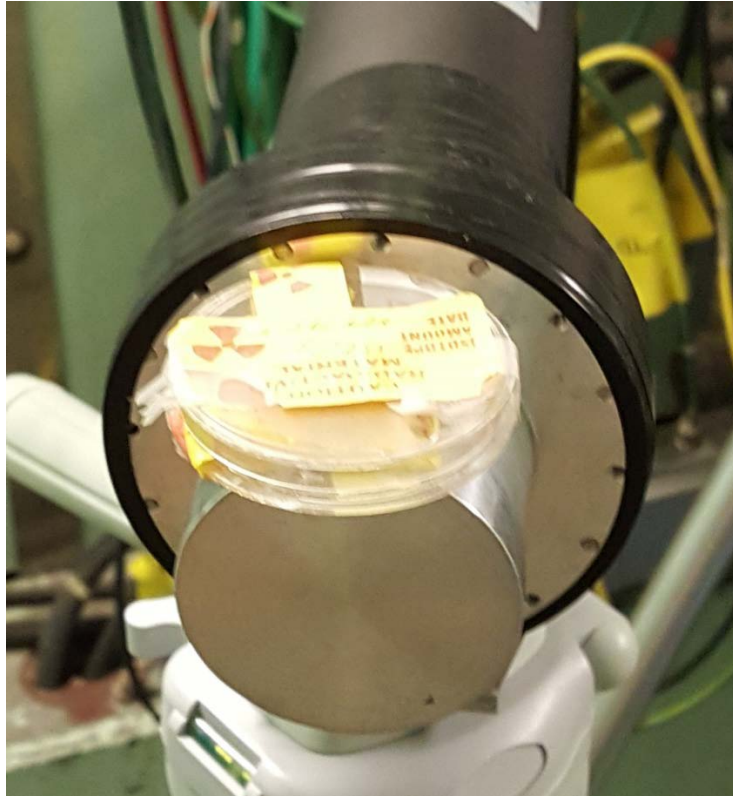
Figure 8. Calibration of one of the EJ-309 detectors for calibration run 2 using the ^{137}Cs source.

Figure 9. The three detectors arranged around a ^{60}Co for the calibration run 3 measurements.

Table 2 details which detector was placed at each position, along with the digital data acquisition (DAQ) channel number.

Table 2. Detector position to DAQ channel for run 3 of the calibration.

EJ-309 Detectors	Calibration Position Around Source (degrees)	Experiment Position from Front of ETA (degrees)	DAQ Channel
Detector 1	0	0	0
Detector 2	120	45	2
Detector 3	240	90	4

3.2 Data Analysis
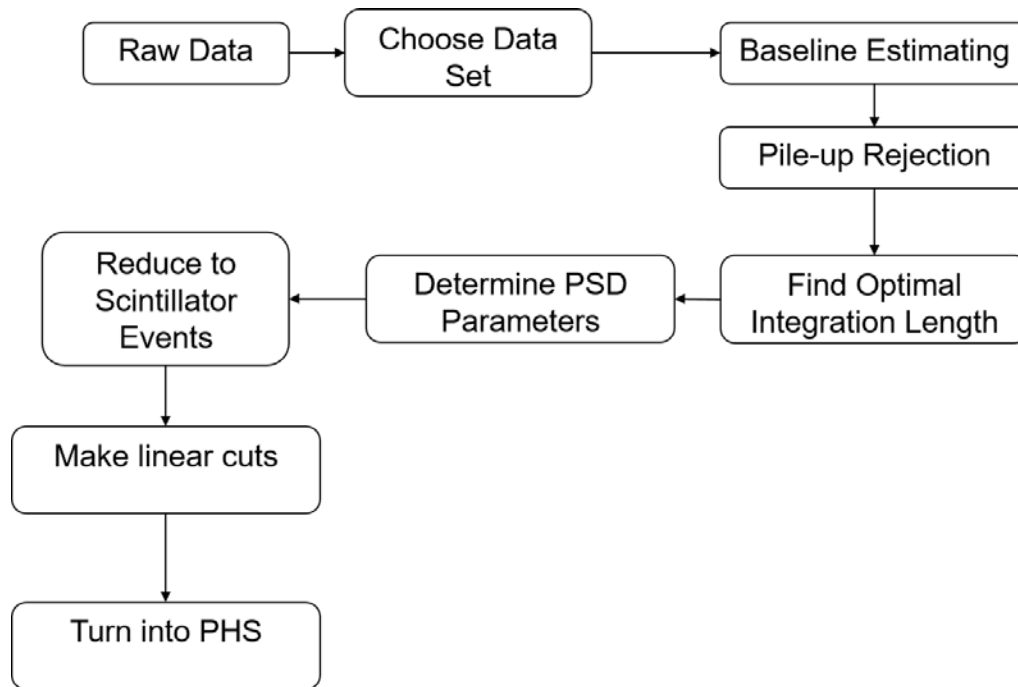
Figure 10. The general signal processing chain used to reduce the raw waveform data into a neutron pulse height spectrum.

The general analysis process is shown in Figure 10. The raw data was collected in previous research [15], and the signal processing steps to turn the raw data into a neutron pulse height spectrum (PHS) were developed in this research. For this process, the raw data was collected from the 88-Inch Cyclotron at Lawrence Berkeley National Laboratory. The following are the key steps in the analysis used:

- A baseline estimating algorithm is run to correct for baseline drift.

- The individual waveforms are run through a pile-up rejection algorithm to remove signals where multiple pulses overlap.

- The optimal integration window is found for the given data set.

- The data is analyzed using several methods of pulse shaped discrimination (PSD) to determine the best parameters for separating the gammas from neutrons.

25

- The data is processed using the parameters found in the previous steps and compressed into the format needed for the creation of the pulse height spectra (PHS) and determine linear cuts for software threshold and PSD value between neutron and gamma peaks.

- PSD is performed to separate the neutrons and gammas for analysis.

- Pulse height cuts are applied to correspond to the channels of complete data collection resulting from a non-linear software threshold.

- The remaining data is turned into a histogram showing the number of neutrons detected at each of the detector's energy channels.

With the data already in the ROOT format, the first step used was to develop the optimal parameters needed to process the data. For this research, the AmBe data was used due to the smaller file sizes and possessing many of the same features as the ETA data. For the calibration data, runs 0 and 1 were ignored due to changing the gain and pre-trigger on the detectors. The data used for the pre-experiment calibration was in Run 2 while the post-experiment calibration data was from Run 3. The following section show the steps used to analyze the raw data using the repository of tools developed by BANG group. The repository used was pulled on August 2017, and subsequent changes to the repository for this research were added to the repository. The specific commands and inputs used to execute each step are shown in Appendix A.

3.2.1 AmBe PSD Parameters

To perform the energy calibration, it is necessary to separate the gamma pulses from the neutron data in the AmBe data. First, it is necessary to determine the parameters needed to fill out the DSP parameter file, as shown in Appendix B. The DSP parameter file contains the necessary detector dependent information to process the waveform data. For all of the data, the time

26

component is given in samples, where one sample equates to 2 ns. The uncalibrated pulse height

is in terms of least significant bits (LSB), where the unit conversion to charge is 20 fC/LSB.

The threshold and smoothing window are determined using the *SCDigitalDaqPostProcessing::developPileupRejectionParameters( )* algorithm. The optimal smoothing window using a center moving average, and the trigger threshold is the threshold on the raw data for the detection of a pulse. This algorithm also passes along the information needed for the baseline subtraction routine that cancels detector baseline drift. An example pile-up event is shown in Figure 11.
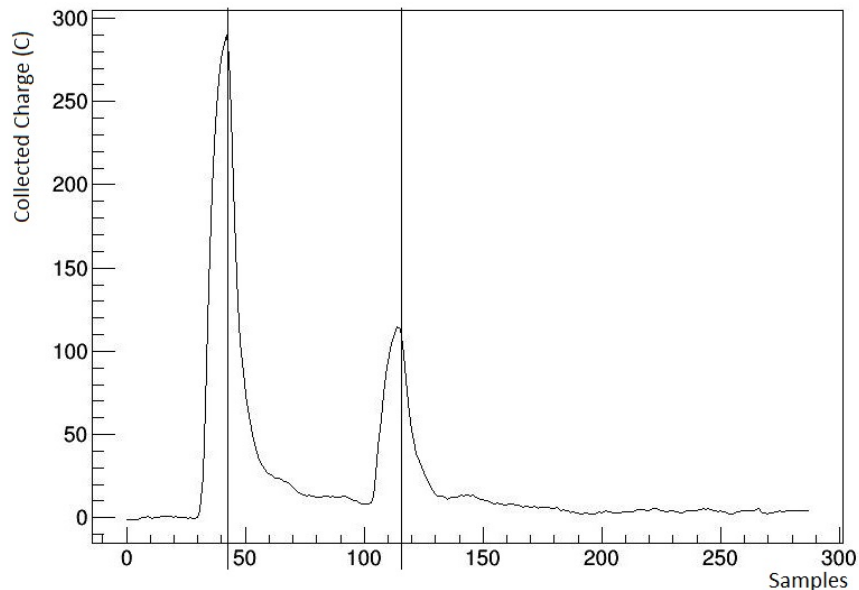
Figure 11. Example pile-up event from the AmBe calibration run 2. Here a smoothing window of 9 samples is used on the channel 0 data, and the integration window for this sample is 150 samples. As the two peaks are within the window, this sample is going to be flagged and thrown out as pile-up during processing.

The smoothing window for the data was determined iteratively by starting with a value of 3 and working to higher values, then looking at the noise level after changing the values and determining if it changed the pulse more than needed. The detection threshold was also determined in this step by picking a threshold that was above the smoothed noise level. It was found that the smoothing window and the threshold were the same for all channels. For the AmBe, the smoothing

window that worked the best for channel 0 was 9 with a threshold of 12. If the smoothing window became larger, the shape of the pulse would begin to distort or the start of the pulse would appear to be cutoff. If the window was too small the noise would distort the pulse end. For the threshold, 12 was used so as to be above the noise while still catching the smaller amplitude pulses.

Once the data was properly smoothed and a threshold determined, the optimal integration window for pulse analysis was determined. The optimal integration window was found qualitatively by comparing the mean pulse height value (mean x in Table 3) of the PSD spectra for the same PSD parameters. The integration windows using a set of PSD values and increasing by 25 samples from 75 to 200.

From comparing the difference in the x mean, which is the average pulse height, the optimal integration window chosen was 150 samples due to the decreasing rate of change in the mean from average pulse height for 125 and 150 samples. The average pulse height and the difference with the last set is shown in Table 3. This set of commands was also run for the clean beam and ETA data and the results were similar.

Table 3. Differences in the average pulse height as the integration window is increased.

Samples	Average Pulse height	Difference
75	5416	
100	5522	106
125	5598	76
150	5653	55
175	5696	43
200	5730	34

The *SCDigitalDaqPostProcessing::calibrateDSP()* algorithm was used to determine the optimal PSD parameters. It uses the raw, unprocessed file and loops over peak and tail windows in user defined steps for user defined minimum and maximum windows to determine the set of PSD parameters with the highest figure of merit as defined in Equation 9 for each channel.

A PSD spectrum was created and FOM was calculated for all sets of PSD values within the user defined range. This allowed for the quantitative determination of which set of parameters had both the best FOM, as defined in Equation 9, and a qualitative determination of which set of values had the greatest degree of separation near the low channel software threshold. The same routine is run again with a smaller window around the optimal parameters from the first run to refine the search space repeating the above analysis methodology. The best values for each parameter using both the tail-to-peak and tail-to-total methods are shown in Table 4. While there is an option to use the 90-10 method, this portion of the programming was not working at the time of analysis.

The PSD plot for AmBe channel 0 using the tail-to-peak method is shown in Figure 12, and the tail-to-total method is shown in Figure 13. The best was defined by the plot which had the best-defined separation at the bin that was closest to the software threshold. Tail-to-Peak is the method that achieves the best results based on the FOM, show in Table 4, and the degree of separation, shown in Figure 12.

Table 4. PSD parameters found by the SCDigitalDaqPostProcessing::calibrateDSP() algorithm for an AmBe source, and the FOM associated with each set.

Tail to Peak Method				
Channel	Peak Window	Tail Offset	Window	FOM
0	18	14	29	1.788
2	23	14	37	1.754
4	19	14	36	1.688
Tail to Total Method				
Channel	Peak Start	Tail Offset	Integration Length	FOM
0	12	15	150	1.167
2	12	15	150	1.119
4	12	15	150	1.049
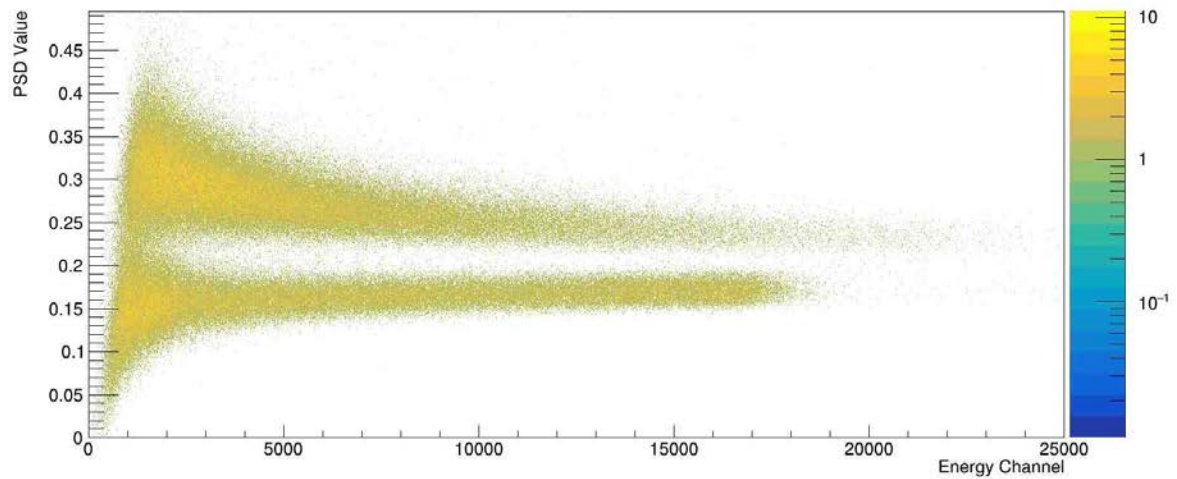
Figure 12. PSD parameter verse energy bin for channel 0 using the tail-to-peak method with AmBe source and the PSD parameters shown in Table 4
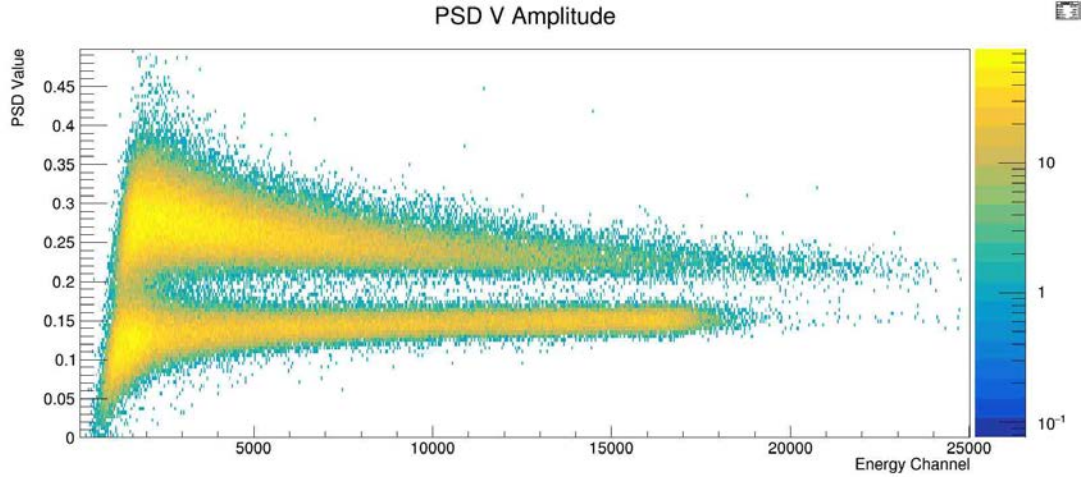
Figure 13. PSD parameter verse energy bin for channel 0 using the tail-to-total method with AmBe source and the PSD parameters from Table 4.

To determine where to perform the linear PSD cuts, a y-projection was used to show the minimum between the neutron and gamma band along the energy channel cut. For the AmBe run 2 data, the cut lines are shown in Table 5 for the different detectors.

Table 5. List of the linear cuts for each channel of the AmBe data.

Detector Channel Number	PSD Cut	Energy Channel Cut
0	0.21	1300
2	0.22	1300
4	0.23	1300
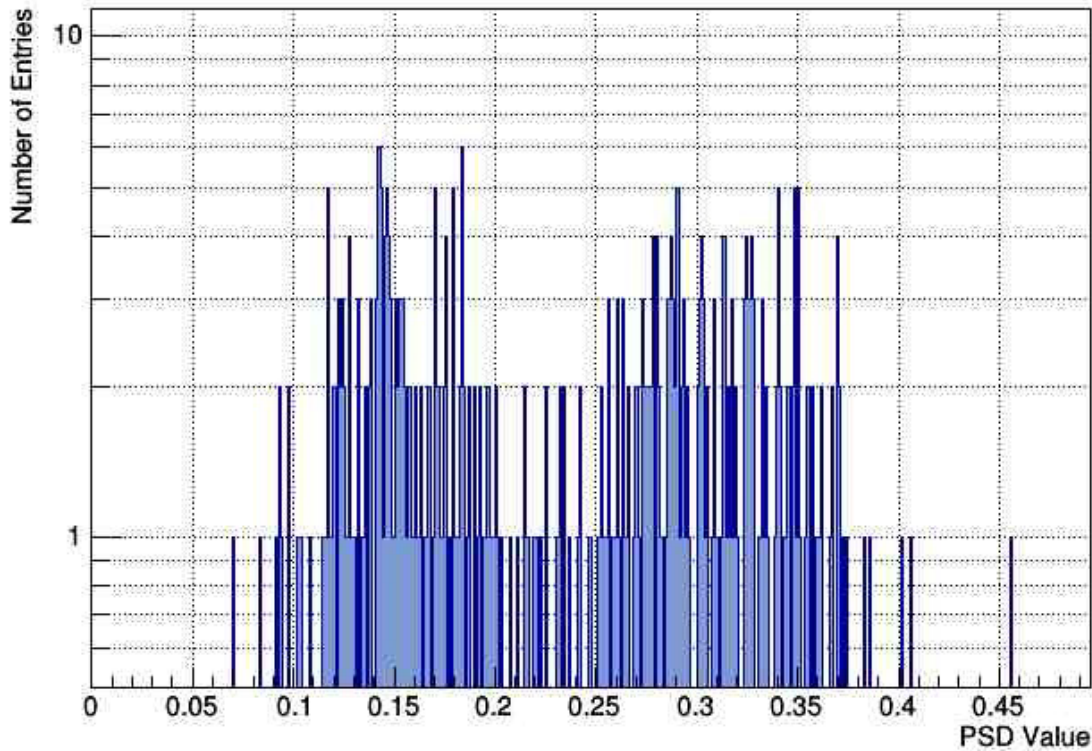
Figure 14. Y-projection for Detector 1 from the AmBe source for the bin covering energy channel 1300-1305.

The next step was to take all of the run 2 and 3 calibration files along with a waveform parameter file created from the parameters above and run the *SCDigitalDaqPostProcessing::reduceFilesToScintillatorEvents()* function to reduce the full waveform tree structure to the *ScintillatorEvent* structure necessary for the calibration, PSD, and pulse-height analysis functions.

The *WFparameterstxt* files, as shown in Appendix B, are necessary for the processing of the data files. This file has the channel number, PSD parameters, pileup rejection parameters, clipping information, and baseline estimating portions that are detector and source specific. This loops over the data and reduce the pulses down from a waveform to a PSD value and an integrated amplitude. This group of commands was continued for all the calibration data files. These files are then combined so that all of detector 1 for each run is in the channel_0_events of the files.

Now, the cuts are applied and the gamma histograms are saved to different files dependent on the channel numbers. The cuts used for AmBe were linear cuts along the PSD value and the pulse height channel for each detector.

This set of commands will take a pulse height spectrum and separate the gamma and neutron spectra based on the linear cut that was applied. The pulse height spectra are then saved with "_gam" or "_neu" specifiers to identify whether the associated histogram is gamma or neutron particles. As ^{60}Co and ^{137}Cs are pure gamma sources, the pulse height spectra is already processed and do not require any cuts.

Next, the calibration files and the simulated calibration files need to be combined into a single file for each. This was run from the command line in the terminal using the *rootcp* command. The commands were repeated for the detectors from channels 2 and 4 as well.

IV. Analysis and Results

In this section, the PSD parameters are finalized, cuts are applied, and the uncalibrated PHS for the clean beam and the full ETA are created and analyzed.

4.1 Apply PSD Parameters

4.1.1 Clean Beam Data

To prepare the data, it is necessary to remove the gamma events from the data. For both the clean beam run 2 and the ETA run 1 data sets, a new set of PSD values were needed. Using the same set of commands from the finding PSD parameters in the AmBe section in Appendix A and *SCDigitalDaqPostProcessing::calibrateDSP(),* the optimized PSD parameters found are shown in Table 6 from the file CleanBeam_002.5.root.

Table 6. PSD parameters found by the *SCDigitalDaqPostProcessing::calibrateDSP()* algorithm for clean beam run 2 data and the FOM associated with each set.

PSD Parameters				
Channel	Peak Window	Tail Offset	Tail Window	FOM
0	16	15	25	1.638
2	14	12	31	1.669
4	12	12	31	1.601

PSD spectra generated using these parameters are shown in Figure 15 – Figure 17 for detectors 1, 2, and 3, respectively. In Figure 15, there are three separate horizontal peaks going from bottom to top where the bottom one is the gamma peak, followed by the neutron peak and then the alpha peak. The alpha peak is created within the detector from some of the fast neutron

absorption by carbon in the detectors, which forms an unstable compound nucleus followed by the emission of alpha particles. The alpha peak is also noticed in the full ETA detector 1 data. The data from detectors 2 and 3 do not contain an alpha peak due to these detectors not being in direct view of the neutron beam and only see scattered neutrons. Those neutrons that are detected at detectors 2 and 3 are lower in energy and hence don't have sufficient energy to cause (n,alpha) reactions. Additionally, as is apparent from Figures 18 and 19 there are much fewer neutrons interacting in detectors 2 and 3.

Figure 15. Detector 1 PSD Spectrum from the clean beam run 2 data using the parameters found in Table 6.

Figure 16. Detector 2 PSD Spectrum from the clean beam run 2 data using the parameters found in Table 6.

Figure 17. Detector 3 PSD Spectrum from the clean beam run 2 data using the parameters found in Table 6.

4.1.2 ETA Data

The *SCDigitalDaqPostProcessing::calibrateDSP()* command was run again with the file

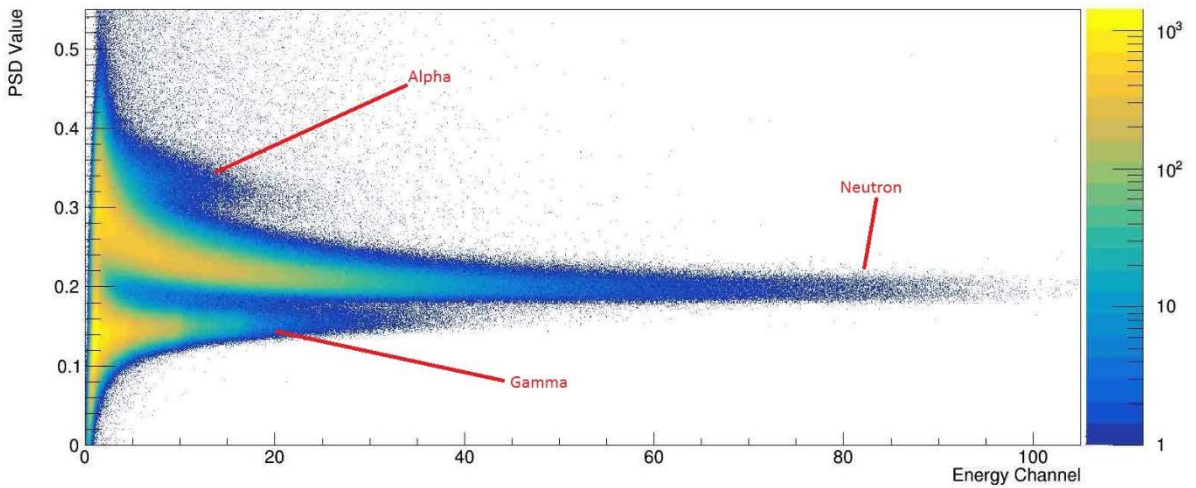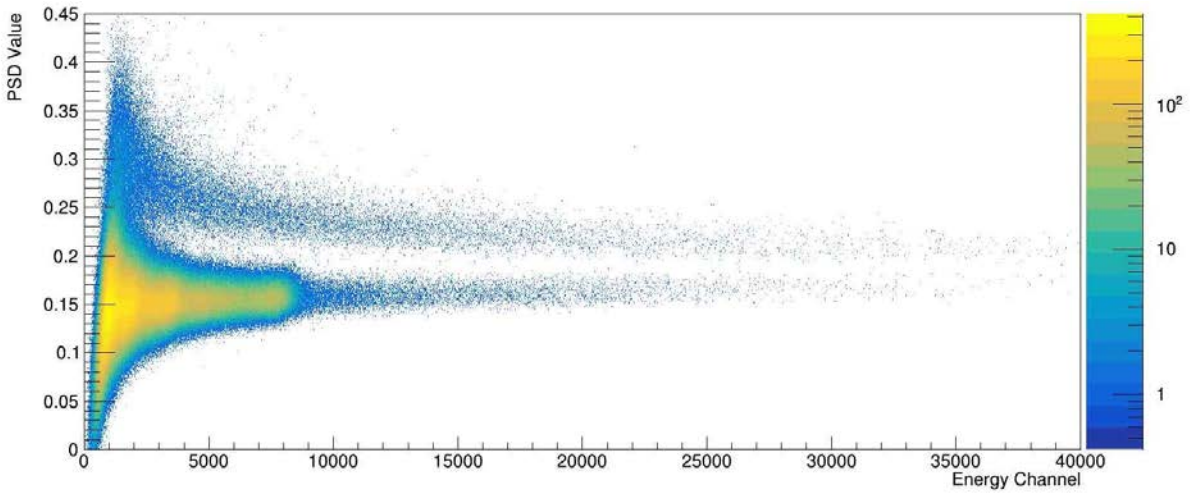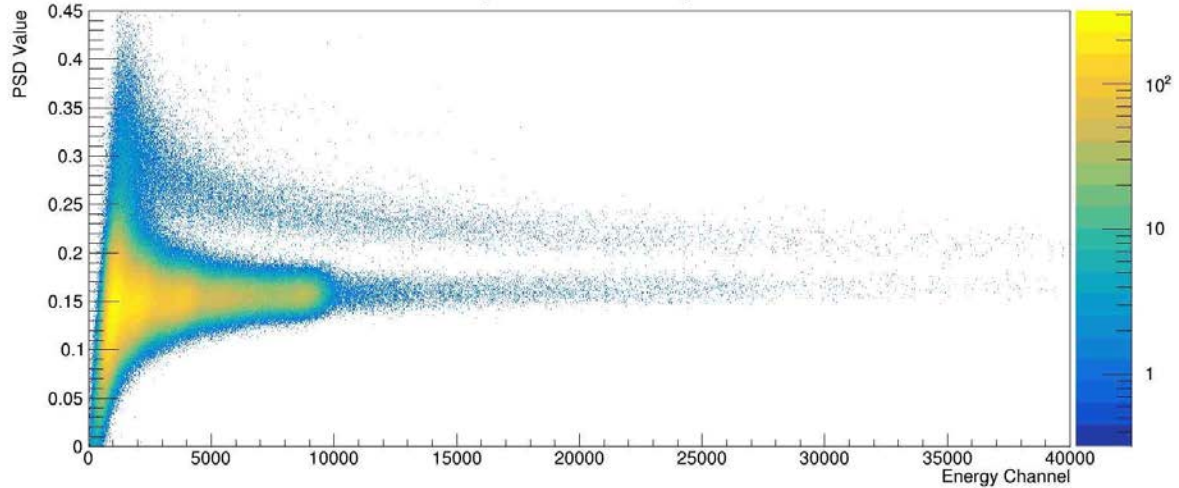ETA_001.4.root and Table 7 shows the parameters broken down by channel for the combined run.

Table 7. PSD parameters found by the *SCDigitalDaqPostProcessing::calibrateDSP()* algorithm for ETA run 1 data and the FOM associated with each set.

PSD Parameters				
Channel	Peak Window	Tail Offset	Tail Window	FOM
0	10	14	28	1.690
2	10	14	28	1.693
4	10	14	28	1.693

Similar to the clean beam, these parameters are used to generate the PSD spectra are shown

in Figure 18 – Figure 20, for detectors 1, 2, and 3, respectively. The alpha peak can be seen in

Figure 18 above both the neutron and gamma peaks. For this run the alpha peak is nothing more

36

than a bump due to being scattered by the ETA. Detectors 2 and 3 are collecting the scatter off of

the ETA from the beam of neutrons hitting it cone part first.
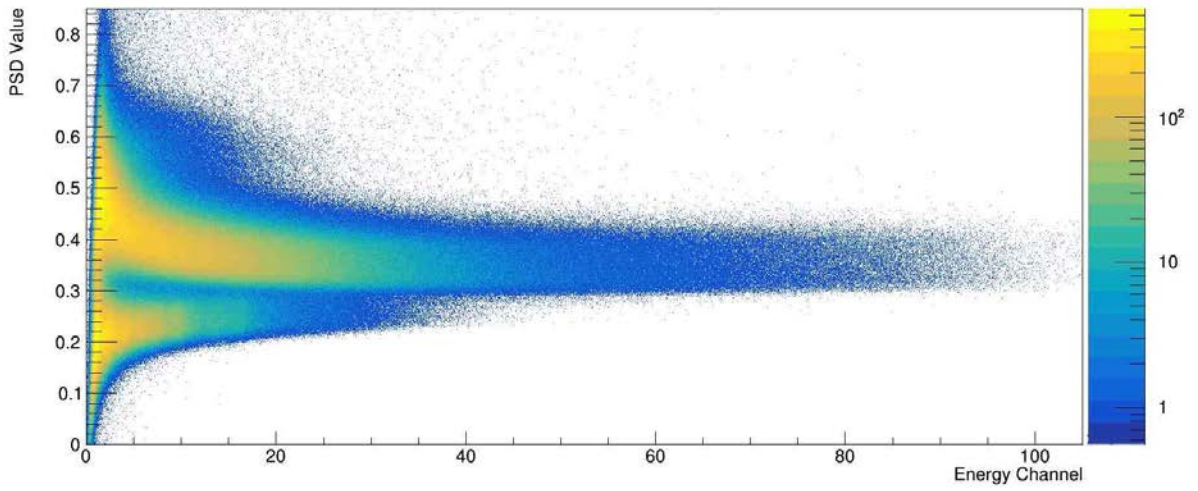
Figure 18. Detector 1 PSD Spectrum from the ETA run 1 data using the parameters in Table 7.
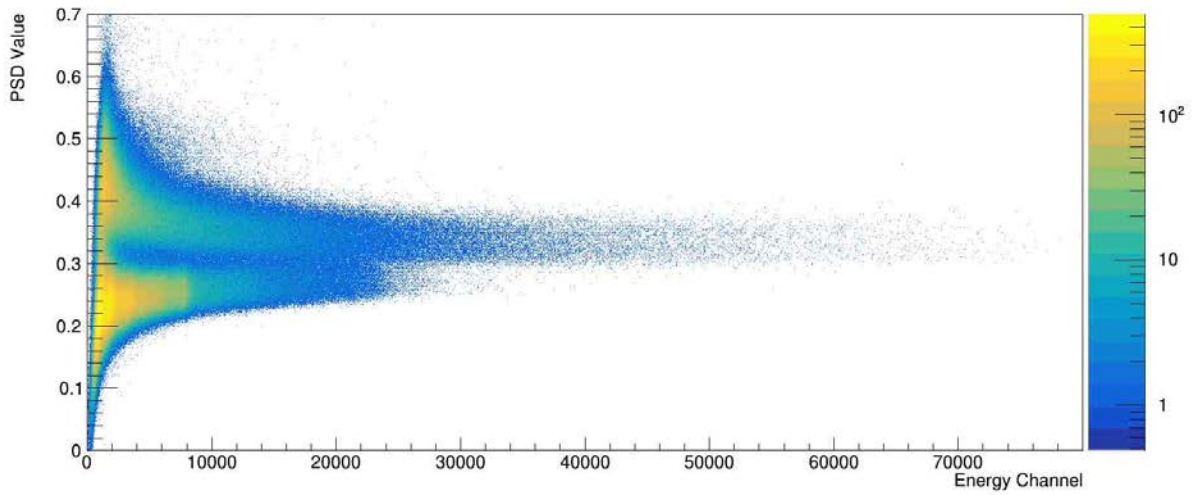
Figure 19. Detector 2 PSD Spectrum from the ETA run 1 data using the parameters in Table 7.
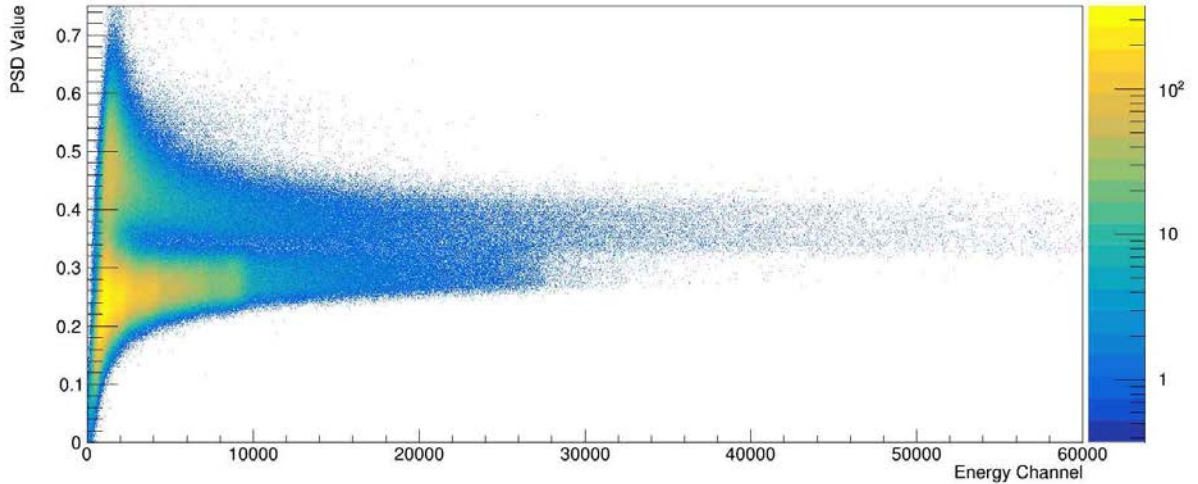
Figure 20. Detector 3 PSD Spectrum from the ETA run 1 data using the parameters in Table 7.

4.2 Pulse Height Spectra

4.2.1 Clean Beam Data

Figure 21 – Figure 23 show the uncalibrated neutron counts per energy channel from the clean beam run 2 data. These are separated by detector and are histograms of counts per energy channel. This is after applying the linear cuts within the function *DDaqPostProcessing::makeDualPhSpectra()*. The linear cuts were found as described in Section 3.2.1. The y-projections of each at the energy channel cut are shown in Appendix C.2. The goal of this function is to create a neutron only spectrum and a gamma only spectrum of the data set of interest. Table 8 shows the cuts for each channel in the data set from the beam only data. As was expected for the clean beam data, detector 1 contains the vast majority of the neutron particles due to detectors 2 and 3 not being in the beam path.

Table 8. List of the linear cuts for each channel of the clean beam Run 2 data.

Detector Channel Number	PSD Cut	Energy Channel Cut
0	0.21	1300
2	0.20	1300
4	0.20	1300
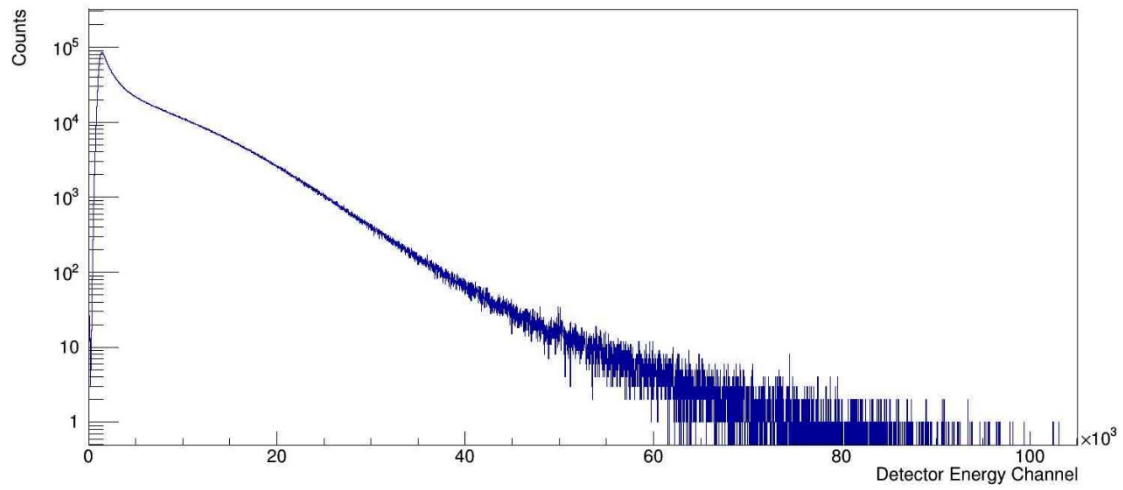
Figure 21. Uncalibrated neutron counts per energy channel for Detector 1 from clean beam run 2 using the cuts from Table 8.

Figure 22. Uncalibrated neutron counts per energy channel for Detector 2 from the clean beam run 2 using the cuts from Table 8.
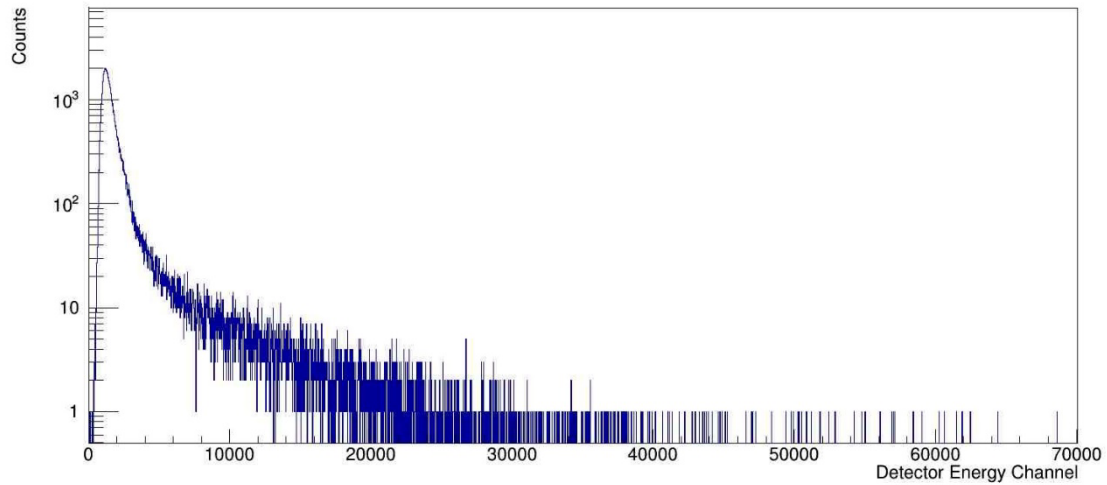
Figure 23. Uncalibrated neutron counts per energy channel for Detector 3 from the clean beam run 2 using the cuts from Table 8.

4.2.2 Full ETA
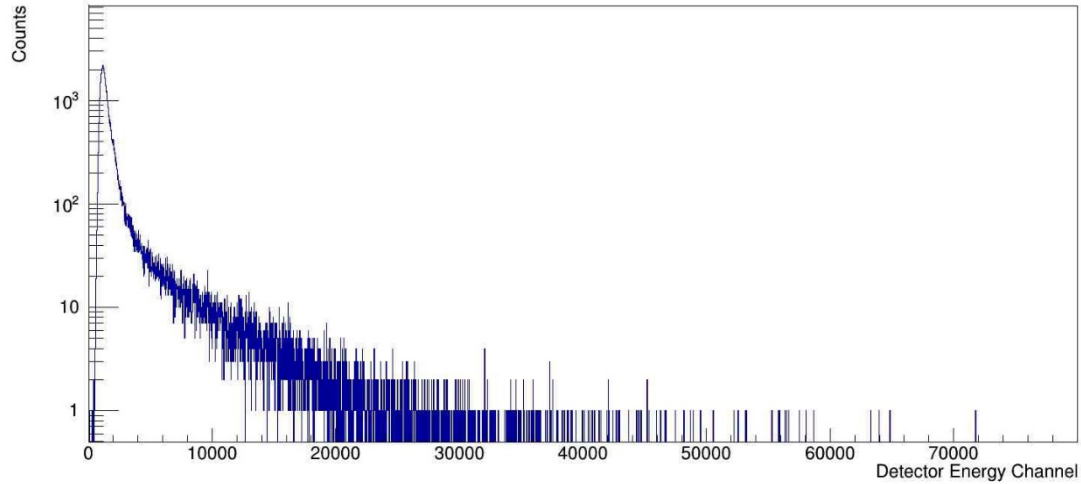
Figure 24 – Figure 26 show the uncalibrated neutron counts per energy channel from the ETA run 1 data separated by detector. This is after applying the linear cuts within the function *DDaqPostProcessing::makeDualPhSpectra()*. The linear cuts were found as described in Section 3.2.1. The y-projections of each at the energy channel cut are shown in Appendix C.3. The goal

40

of this function is to create a neutron only spectrum and a gamma only spectrum of the data set of interest. Table 9 shows the cuts for each channel in the data set from the full ETA data.

The ETA did increase the scatter of neutrons into detectors 2 and 3 from the main beam as expected. More analysis is needed to determine if the expected spectrum was created with the ETA.

Table 9. List of the linear cuts for each channel of the ETA data.

Detector Channel Number	PSD Cut	Energy Channel Cut
0	0.31	1300
2	0.32	1300
4	0.35	1300

Figure 24. Uncalibrated neutron counts per energy channel for Detector 1 from the ETA run 1 using the cuts from Table 9.
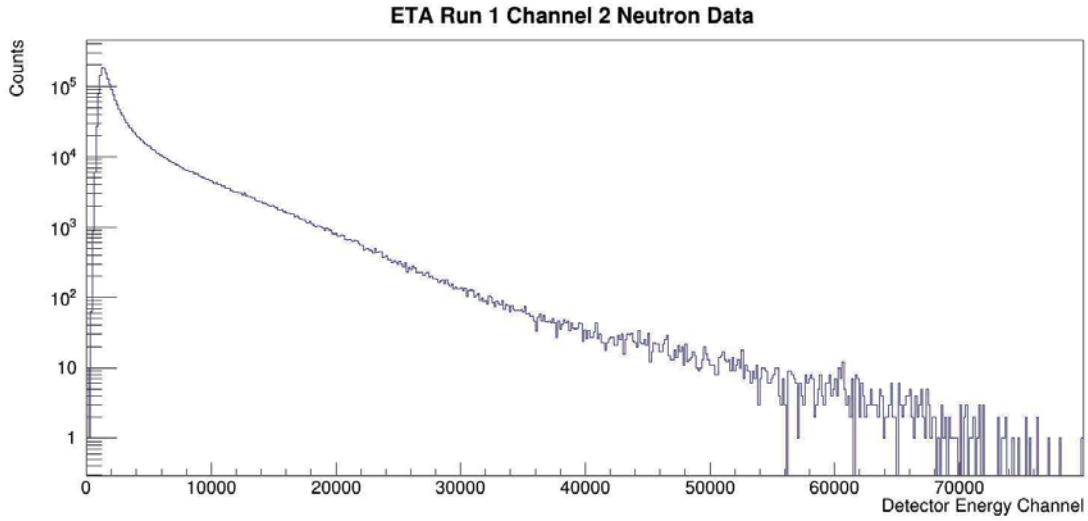
Figure 25. Uncalibrated neutron counts per energy channel for Detector 2 from the ETA run 1 using the cuts from Table 9.
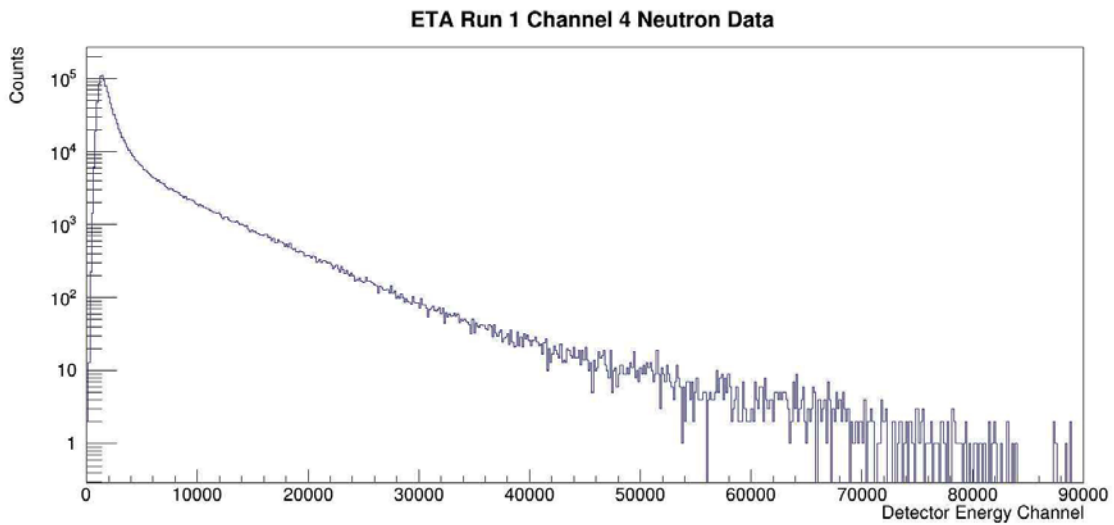
Figure 26. Uncalibrated neutron counts per energy channel for Detector 3 from the ETA run 1 using the cuts from Table 9.
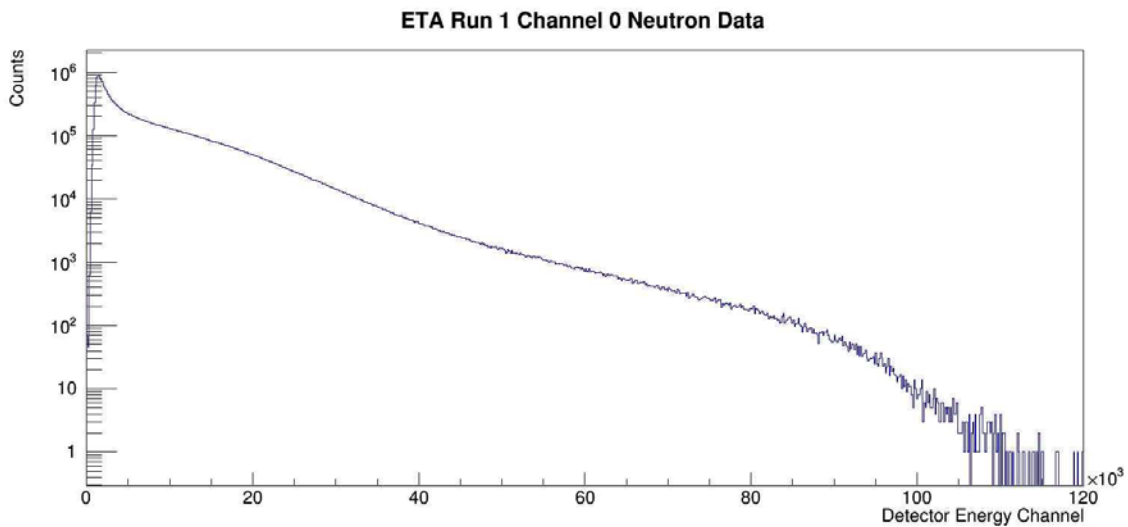
V. Conclusions and Future Work

This research modified an existing code and created an analysis chain. The purpose was to determine the neutron pulse height spectrum from the Lawrence Berkeley National Laboratory 88-Inch Cyclotron after spallation with a tantalum target and collect the scattered spectrum off the ETA with EJ-309 liquid organic scintillators. The following section discusses, in detail, some conclusions that were drawn, specifically in reference to the objectives posed in Section 1.2.1.

5.1 Conclusions

In this research, full waveform data was taken from the Lawrence Berkeley National Laboratory 88-Inch Cyclotron for the ETA experiment. This data was then run through various algorithms to determine the optimal PSD method and the optimal parameters for the integration window, smoothing window, and PSD parameters. The data was then processed and a PSD spectrum was created. With the PSD spectrum, the linear cuts along the PSD value and the energy channels were determined for the data sets. With the linear cuts, the neutrons were separated from the gammas and placed into histograms showing the counts verse energy channel.

Based on the analysis of the signal data, using the full waveform data does provide better flexibility in determining the optimal PSD parameters and adapting and modifying PSD methods and window definitions, which in turn likely means better discrimination between gammas and neutrons at low pulse heights. This research appears to have been able to get a better PSD than previously found. Previous work only looked at using the Tail-to-Total method and for the case of this research it was found the Tail-to-Peak method gave us a better discrimination, as seen in Figure 12 and Figure 13. Due to using the full waveform data, this research was also able to better home in on the best PSD parameters, thereby allowing this research to better discriminate between gamma and neutron particles at low pulse heights.

5.2 Recommendations for Future Research

The calibration was not completed for this research, and this would be required for a direct comparison between this work analyzing and previous analysis. Along with the calibration, the comparison needs to be made to determine if any drift occurred in the detectors from either equipment heating up or from neutron activation of materials.

For this research, only linear cuts were applied. This is due to difficulties occurring when the Gaussian fitting routine was used. The clean beam and ETA data would both be improved by applying a fitted cuts routine to the data for the PSD cuts since there is overlap in the two distributions at low pulse heights

Another part of the coding that was not working correctly was the 90-10 PSD method. It would be interesting to know if using this method would produce better PSD results. This method should have worked very well based on literature; however, when it was looked at for this research the PSD appeared to have been clipped. The root cause of this was not determined in this research.

The only data analyzed was the clean beam data and the full ETA. There are still several sets of full waveform data from the buildup of materials to be analyzed. These materials are bismuth, the aluminum case, praseodymium, silicon, and tungsten.

The natural progression of this research would also be to unfold the calibrated PHS. The unfolded neutron spectra could then be compared to an MCNP or a GEANT4 simulation of the expected spectrum. Differences may point to gaps in nuclear data for the neutron energies and reaction channels examined in this experiment.

Appendix A

A.1 Energy Calibration

A.1.1 Develop Pile-up Rejection Parameters

After typing the commands, a canvas will appear, similar to Figure 11, and the user will be given the option to change the smoothing window and the threshold. The 0 and 10000 are arbitrary pulses to look at for pile-up. The final step is repeated for channels 2 and 4 as well. The goal for this portion of the code is to determine the triggering threshold for finding the pulses above the noise and determining the smoothing window based on the center moving average.

```
>>SCDigitalDaqPostProcessing ambe
>>ambe.loadFile("AmBe_002.0.root")
>>ambe.developPileupRejectionParameters(0,10000,0,9,12)
```

A.1.2 Develop Optimal Integration Window

This function *DigPSDAnalysis::getTailToPeakHist()* requires the data file to be processed already, which is addressed by the first set of commands to process and combine the two AmBe Run 2 files into one processed TTree. The goal of the first group of commands is to combine the run files into one so there is only one file per run. The second group of commands is to create a PSD spectrum based on the parameters you give the algorithm.

```
>>SCDigitalDaqPostProcessing part1
>>part1.loadFile("AmBe_002.0.root")
>>part1.processTreesForTailToPeakAnalysis("test1.root")
>>SCDigitalDaqPostProcessing part2
>>part2.loadFile("AmBe_002.1.root")
>>part2.processTreesForTailToPeakAnalysis("test2.root")
```

```
>>.q

>>hadd ambetree.root test1.root test2.root

>>root

>>DigPSDAnalysis psd

>>psd.loadFile("ambetree.root")

>>psd.getTailToPeakHist(0,16,28,16,200,-1)

>>TBrowser a
```

A.1.3 Develop Optimal PSD Parameters

The process to determine the optimal PSD method and the associated parameters uses the *SCDigitalDaqPostProcessing::calibrateDSP()* function. This set of commands requires unprocessed files. The first set of user prompts are to determine the channels analyzed, PSD method, and common starting point. The user inputs the channels to ignore in this process, the PSD method, and the triggering threshold for the top part of the inputs. The algorithm then, processes the data in the channels and asks for the user to define the minimum and maximum values for the window of the peak, the offset for the tail to start and the window of the tail for the pulse. The algorithm then incrementally loops over the values to create a PSD spectrum for all combinations within the windows. The code also calculated the Figure of Merit and finds the one with the highest FOM, the code defines that set of parameters as the optimal PSD.

```
>>SCDigitalDaqPostProcessing test

>>test.loadFilepost.loadFile("CleanBeam_002.3.root")

>>test.calibrateDSP()

Are there any channels present that should be ignored while tuning?

(yes,no):

>>yes

enter the channel number

>>2
```

Is there another channel to ignore?

>>yes

enter the channel number

>>4

Is there another channel to ignore?

>>yes

enter the channel number

>>14

Is there another channel to ignore?

>>no

What psd method would you like to use?

Tail to Peak: 1

Tail to Total: 2

90 10 Delta T: 3

>>1

Would you like to use a common start or one determined from a leading

edge discriminator?

If you would like to use leading edge, enter -1*threshold in bits

If you would like to use a common start please reference the plot and

enter the sample number

>>-16

Enter Short Gate Min.(8)

>>8

Enter Short Gate Max.(28)

>>28

```
Enter Tail Min.(20)

>>20

Enter Tail Max.(60)

>>60

Enter tailOffsetMin.(6)

>>6

Enter tailOffsetMax.(24)

>>24

Enter Integration Length(200)

>>150

The results obtained were


The best figure of merit is 1.76518

The best parameters appear to be

Peak Window = 12

Tail Window = 30

Tail Offset = 15
```

Round 2 is to determine a finer window for determining the parameters.

```
Enter Short Gate Min.(8)

>>8

Enter Short Gate Max.(28)

>>18

Enter Tail Min.(20)

>>24
```

```
Enter Tail Max.(60)

>>36

Enter tailOffsetMin.(6)

>>6

Enter tailOffsetMax.(24)

>>24

Enter Intergration Length(200)

>>150

The best figure of merit is 1.77612

The best parameters appear to be

Peak Window = 16

Tail Window = 28

Tail Offset = 15
```

A.1.4 File Names for the Calibration Files

Table 10. Combined file names for the calibration root files.

Run 2			
AmBe	AmBe_002.0.root	AmBe_002.0_SE.root	AmBeRun2_SE.root
	AmBe_002.1.root	AmBe_002.1_SE.root	
Co60	Co60_002.0.root	Co60_002.0_SE.root	Co60Run2_SE.root
	Co60_002.1.root	Co60_002.1_SE.root	
Cs137	Cs137_002.0.root	Cs137_002.0_SE.root	Cs137Run2_SE.root
	Cs137_002.1.root	Cs137_002.1_SE.root	
Run 3			
AmBe	AmBe_003.0.root	AmBe_003.0_SE.root	AmBeRun3_SE.root
	AmBe_003.1.root	AmBe_003.1_SE.root	
Co60	Co60_003.0.root	Co60_003.0_SE.root	Co60Run3_SE.root
	Co60_003.1.root	Co60_003.1_SE.root	
Cs137	Cs137_003.0.root	Cs137_003.0_SE.root	Cs137Run3_SE.root
Background	Background_003.0.root	Background_003.0_SE.root	BackgroundRun3_SE.root

A.1.5 Reduce Files to Scintillator Events

There are two different methods for getting the scintillator events and combine files by source or run. This batch of commands also separates the various channels so the information is able to be processed correctly. Finally, the files from the various runs are merged together. For the AmBe data, the following lines were written in the ROOT command line:

```
>>SCDigitalDaqPostProcessing post

>>post.loadFile("AmBe_002.0.root")

>>post.reduceToScintillatorEvent("AmBe_002.0_SE.root","WFparameterstx"

)

Or:

>>SCDigitalDaqPostProcessing post

>>post.reduceFilesToScintillatorEvents("names.txt"," WFparameterstxt")
```

Combine files so there is one file per expermiment phase:

```
>>Had AmBeRun2_SE.root AmBe_002.0_SE.root AmBe_002.1_SE.root
```

A.1.6 Make Pulse Height Spectra

The function *DDaqPostProcessing::makeDualPhSpectra()* takes the data file that has been processed, applies the linear cuts in the x and y direction, then creates a PHS for the gammas and neutrons. The commands are as follows for the AmBe example:

```
>>DDaqPostProcessing test

>>test.loadFile("AmBe_2_Total_SE.root")

What is the tree name?

>>channel_0_events

Tree Name : channel_0_events

>> test.makeDualPhSpectra("Spectra_AmBe_run2_0.root")

Please input the linear psd cut value:

>>.18
```

For the Cs and Co, since they are pure gamma sources, they use a slightly different set of commands. The end result is the same where you will now have a PHS.

```
>>DDaqPostProcessing Cs

>>Cs.loadFile("Cs137Run2_SE.root")

What is the tree name?

>>channel_0_events

>>Cs.getPhSpectrum()

>>TBrowser a

Save the PhSpectrum_0 as Spectra_Cs137_run2_0.root


>>DDaqPostProcessing Co

>>Co.loadFile("Co60Run2_SE.root")

What is the tree name?

>>channel_0_events

>>Co.getPhSpectrum()

>>TBrowser a

Save the PhSpectrum_0 as Spectra_Co60_run2_0.root
```

Appendix B

B.1 WFParametertxt file for Calibration data

```
//#

15 0

/#

0

0 -12 18 14 29 150

1 9 10

0 10

//#

15 0

/#

2

0 -12 23 14 37 150

1 9 10

0 10

//#

15 0

/#

4

0 -12 19 14 36 150

1 9 10

6 10
```

B.2 WFParametertxt file for CleanBeam data

```
//#

12 0

/#

0

0 -12 16 15 28 150

1 9 12

0 12

//#

12 0

/#

2

0 -12 16 15 28 150

1 9 12

0 12

//#

12 0

/#

4

0 -12 16 15 28 150

1 9 12

0 12
```

B.3 WFParametertxt file for ETA data

```
//#

12 0

/#

0

0 -12 10 14 36 150

1 9 12

0 12

//#

12 0

/#

2

0 -12 14 12 31 150

1 9 12

0 12

//#

12 0

/#

4

0 -12 12 12 31 150

1 9 12

0 12
```
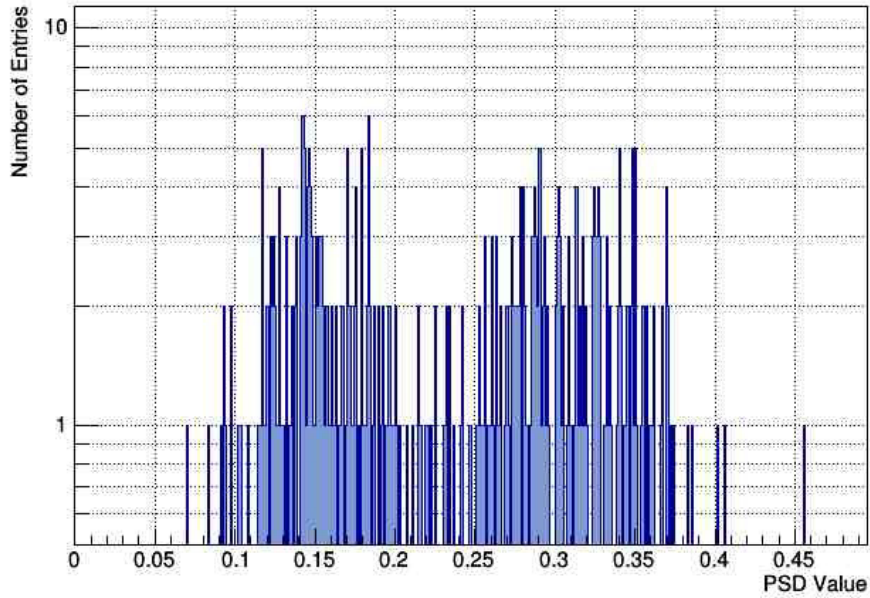
Appendix C

C.1 Y-Projections for AmBe Data

Figure 27. Y-projection for Detector 1 from the AmBe source for the bin covering energy channel 1300-1305.
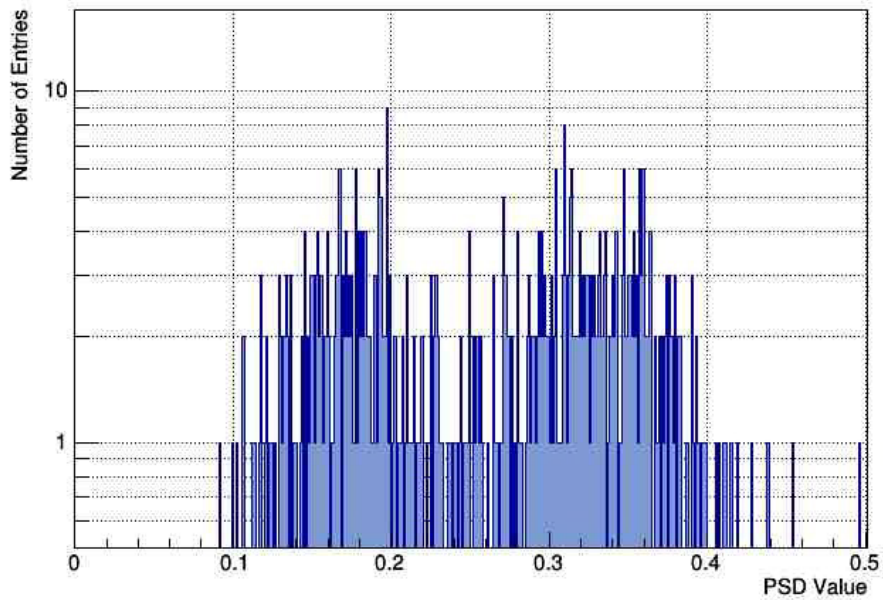

Figure 28. Y-projection for Detector 2 from the AmBe source for the bin covering energy channel 1300-1305.
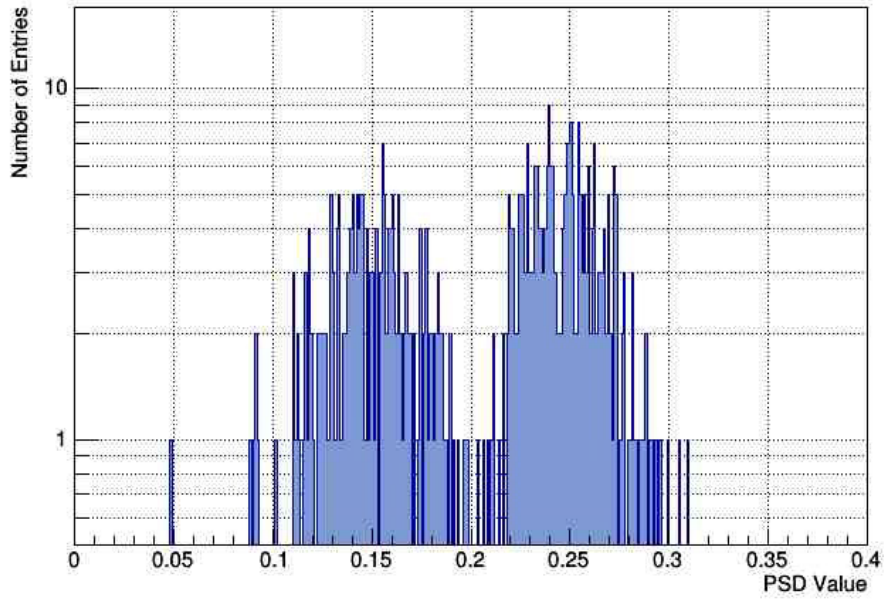
Figure 29. Y-projection for Detector 3 from the AmBe source for the bin covering energy channel 1300-1305.
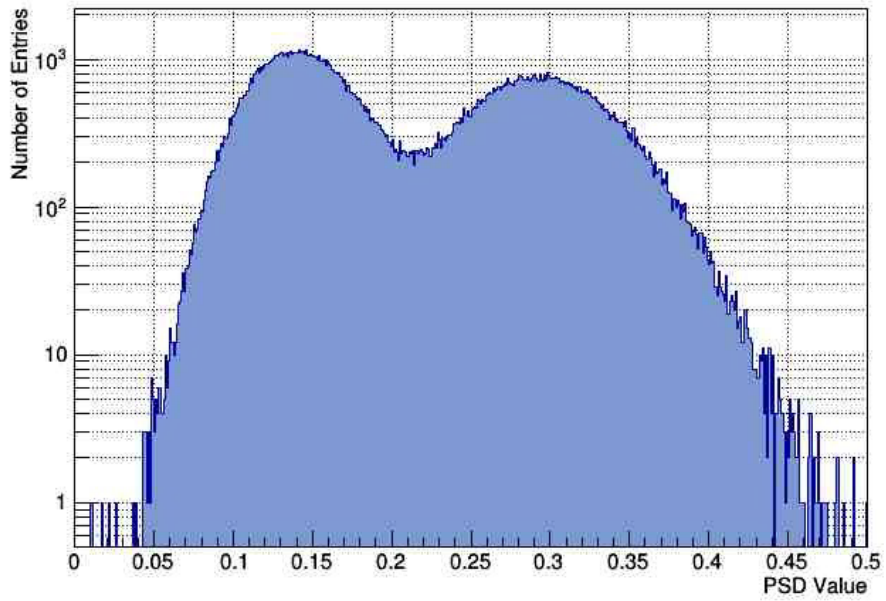
C.2 Y-Projections for Clean Beam Data

Figure 30. Y-projection for Detector 1 from the clean beam source for the bin covering energy channel 1305-1320.
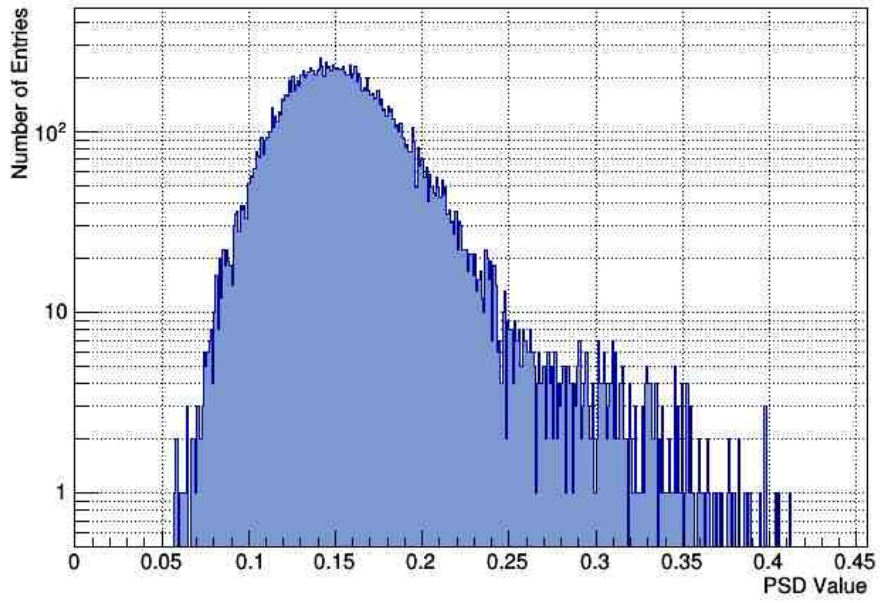
Figure 31. Y-projection for Detector 2 from the clean beam source for the bin covering energy channel 1305-1320.
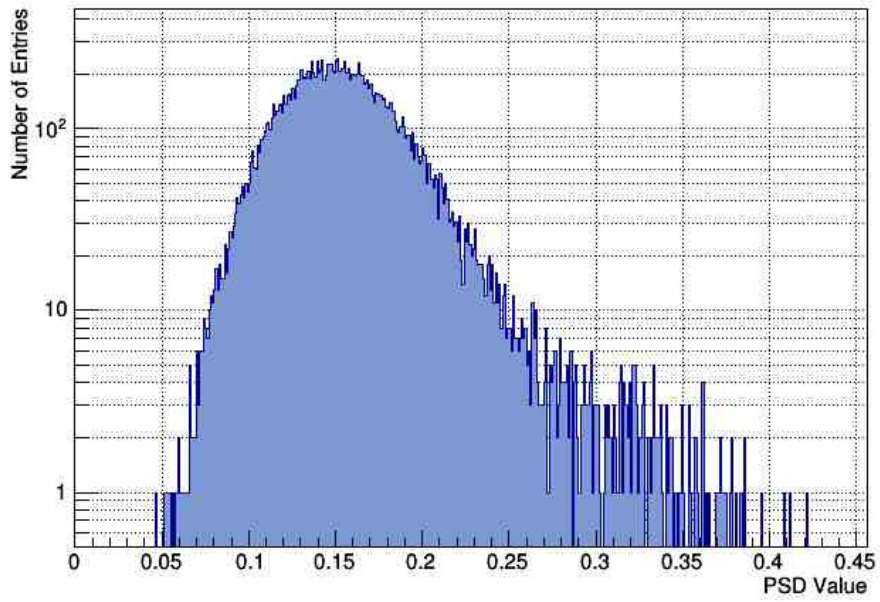

Figure 32. Y-projection for Detector 3 from the clean beam source for the bin covering energy channel 1305-1320.

C.3 Y-Projections for ETA Data

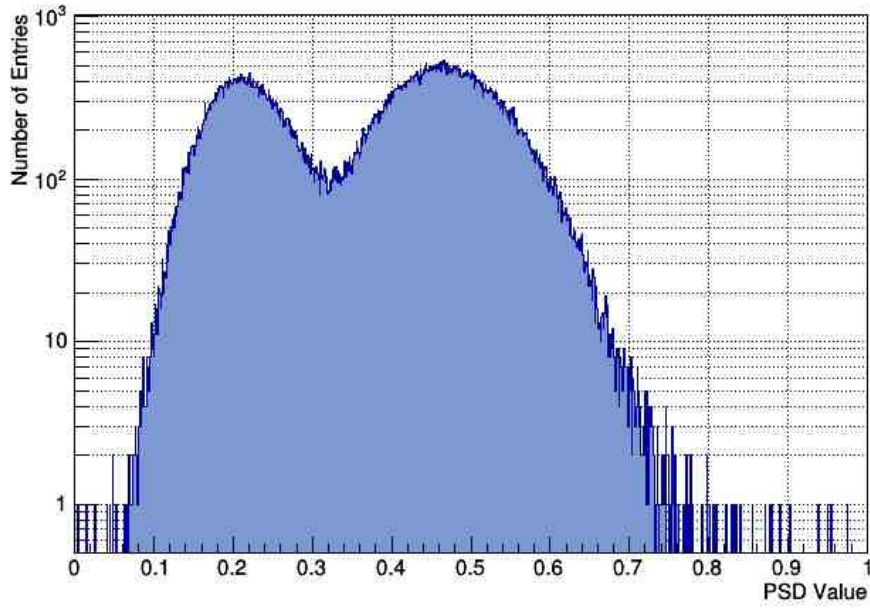
Figure 33. Y-projection for Detector 1 from the ETA source for the bin covering energy channel 1305-1320.
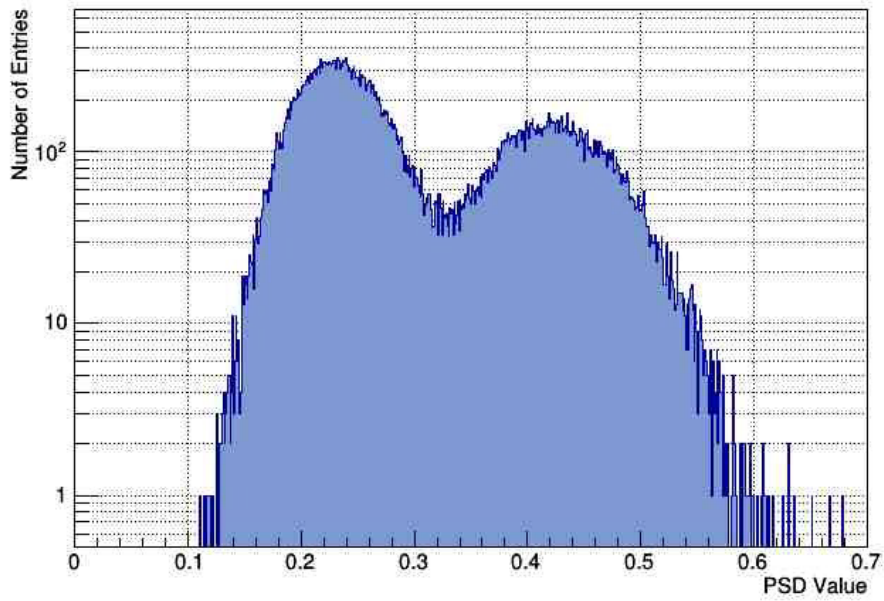

Figure 34. Y-projection for Detector 2 from the ETA source for the bin covering energy channel 1305-1320.
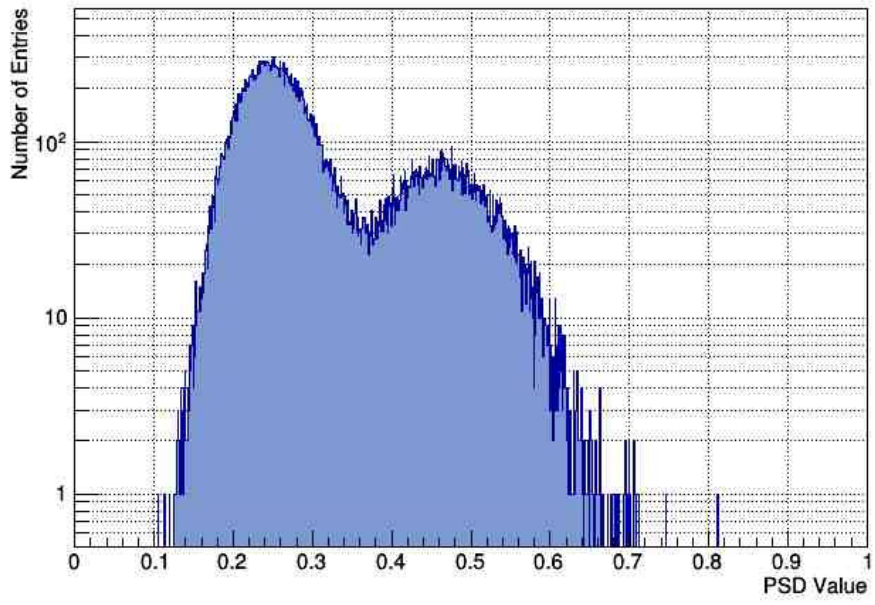
Figure 35. Y-projection for Detector 3 from the ETA source for the bin covering energy channel 1305-1320.

References

[1]   "Stockpile Stewardship Program," *National Nuclear Security Administration*. [Online]. Available: https://wci.llnl.gov/science/stockpile-stewardship-program.

[2]   B. Tarter, "Annual Certification Takes a Snapshop of Stockpile's Health," *Sci. Technol. Rev.*, August, pp. 4–10, 2001.

[3]   W. H. Goldstein, "Lawrence Livermore National Laboratory's Role and Contributions to the Nuclear Security Enterprise," *Hear. Subcomm. Strateg. Forces Comm. Armed Serv. U.S Senat.*, 2014.

[4]   Joe Biden, "The President's Nuclear Vision," *Wall Str. J.*, June, p. 80, 2010.

[5]   Joint Defense Science Board/Threat Reduction Advisory Comittee Task Force, "The Nuclear Weapons Effects National Enterprise," June, 2010.

[6]   B. L. R. Binders, "Nuclear Data Needs and Capabilities for Applications," 2015.

[7]   M. B. Chadwick *et al.*, "ENDF/B-VII.1 Nuclear Data for Science and Technology: Cross Sections, Covariances, Fission Product Yields and Decay Data," *Nucl. Data Sheets*, vol. 112, no. 12, pp. 2887–2996, 2011.

[8]   K.-H. Schmidt and B. Jurado, "General Description of Fission Observables," *Data Bank NEA/DB/DOC*, no. 1, p. 1, 2014.

[9]   D. R. Nethaway and G. W. Barton, "A Compilation of Fission Product Yields in use at the Lawrence Livermore Labratory," *UCRL-51458*, p. 106, 1973.

[10]   Y. Yi *et al.*, "Fission Product Yields from 19.1 MeV Neutron Induced Fission of 238 U," *Commun. Nucl. Data Prog. No.25*, vol. 25, no. 25, pp. 1–3, 2001.

[11]   M. E. Gooden *et al.*, "Energy Dependence of Fission Product Yields from 235U, 238U and 239Pu for Incident Neutron Energies Between 0.5 and 14.8 MeV," *Nucl. Data Sheets*, vol. 131, pp. 319–356, 2016.

[12]   S. Nagy, K. F. Flynn, J. E. Gindler, J. W. Meadows, and L. E. Glendenin, "Mass Distributions in Monoenergetic-Neutron-Induced Fission of U238," *Phys. Rev. C*, vol. 17, no. 1, pp. 163–171, 1978.

[13]   D. W. Heikkinen, "RTNS-II OPERATIONAL SUMMARY," 1988.

[14]   "Alternative Source for Neutron Generation," 2012. [Online]. Available: https://www.sbir.gov/sbirsearch/detail/372834.

[15]   J. Bevins, "Targeted Modification of Neutron Energy Spectra for National Security Applications," University of California, Berkeley, 2017.

[16]   J. P. Meulders, P. Leleux, P. C. Macq, and C. Pirart, "Fast Neutron Yields and Spectra from Targets of Varying Atomic Number Bombarded with Deuterons from 16 to 50 MeV (for Radiobiology and Radiotherapy)," *Phys. Med. Biol.*, vol. 20, no. 2, pp. 235–243, 1975.

[17]   G. F. Knoll, *Radiation Detection and Measurement*, 4th Edition. pp. 1–860, 2010.

[18]   E. E. Lewis and W. F. Miller, *Computational Methods of Neutron Transport*. 1984.

[19]   K. S. Krane and D. Halliday, *Introductory Nuclear Physics*, 3rd ed. Wiley & Sons, 1988.

[20]   J. R. Copley and T. J. Udovic, "Neutron Time-of-Flight Spectroscopy," *J. Res. Natl. Inst. Stand. Technol.*, vol. 98, no. 1, pp. 71–87, 1993.

[21]   A. Donzella *et al.*, "A Proton Recoil Telescope for Neutron Spectroscopy," *Nucl. Instruments Methods Phys. Res. Sect. A Accel. Spectrometers, Detect. Assoc. Equip.*, vol. 613, no. 1, pp. 58–64, 2010.

[22]   T. J. Langford *et al.*, "Fast Neutron Detection with a Segmented Spectrometer," *Nucl. Instruments Methods Phys. Res. Sect. A Accel. Spectrometers, Detect. Assoc. Equip.*, vol. 771, pp. 78–87, 2015.

[23]   Marsh J. W., Thomas D. J., and Burke M., "High Resolution Measurements of Neutron Energy Spectra from Am-Be and Am-B Neutron Sources," *Nucl. Instruments Methods Phys. Res. A*, vol. 366, no. 95, pp. 340–348, 1995.

[24]   A. Mattera *et al.*, "Measurement of the Energy Spectrum from the Neutron Source Planned for IGISOL," *Eur. Res. Infrastructures Nucl. Data Appl. Work.*, June 2012, pp. 1–8, 2013.

[25]   N. P. Luciano, "A High-Energy Neutron Flux Spectra Measurement Method for the Spallation Neutron Source," 2012.

[26]   J. Sandberg, "Determination of Particle Flux Spectra with Multireaction Activation Detectors," *Acta Polytech. Scand.*, vol. 146, 1984.

[27]   S. Sen *et al.*, "Determination of Neutron Energy Spectrum at KAMINI Shielding Experiment Location," *Appl. Radiat. Isot.*, vol. 115, pp. 165–171, 2016.

[28]   Y. H. Chen *et al.*, "Unfolding the Fast Neutron Spectra of a BC501A Liquid Scintillation

Detector Using GRAVEL Method," *Sci. China Physics, Mech. Astron.*, vol. 57, no. 10, pp. 1885–1890, 2014.

[29]   C. C. Lawrence, "Neutron Spectrum Unfolding with Organic Scintillators for Arms-control Verification," p. 210, 2014.

[30]   C. C. Lawrence, A. Enqvist, M. Flaska, S. A. Pozzi, and F. D. Becchetti, "Comparison of Spectrum-Unfolding Performance of (EJ315) and (EJ309) Liquid Scintillators on Measured 252Cf Pulse-Height Spectra," *Nucl. Instruments Methods Phys. Res. Sect. A Accel. Spectrometers, Detect. Assoc. Equip.*, vol. 729, August, pp. 924–929, 2013.

[31]   M. Matzke, "Propagation of Uncertainties in Unfolding Procedures," *Nucl. Instruments Methods Phys. Res. Sect. A Accel. Spectrometers, Detect. Assoc. Equip.*, vol. 476, no. 1–2, pp. 230–241, 2002.

[32]   M. Matzke, "Unfolding of Pulse Height Spectra: The HEPRO Program," *Phys. Tech. Bundesanstalt*, vol. 19, 1994.

[33]   M. Matzke, "The HEPROW Program System," 2003.

[34]   M. Reginatto and P. Goldhagen, "MAXED, A Computer Code for the Deconvolution of Mutilsphere Neutron Spectrometer Data Using the Maximum Entropy Method," 1998.

[35]   N. R. Tsoulfanidis, *Measurement and Detection of Radiation*, 2nd ed. Taylor & Francis, 1995.

[36]   W. Conshohocken, "Standard Guide for Application of Neutron Spectrum Adjustment Methods in Reactor Surveillance , E 706 (IIA) 1," *Nucl. Technol.*, vol. 12, no. September,

pp. 1–10, 2002.

[37] D. A. Barkauskas and D. M. Rocke, "A General-Purpose Baseline Estimation Algorithm for Spectroscopic Data," vol. 42, no. 1, pp. 115–125, 2009.

[38] I. A. Pawełczak, S. A. Ouedraogo, A. M. Glenn, R. E. Wurtz, and L. F. Nakae, "Studies of Neutron-γ Pulse Shape Discrimination in EJ-309 Liquid Scintillator Using Charge Integration Method," *Nucl. Instruments Methods Phys. Res. Sect. A Accel. Spectrometers, Detect. Assoc. Equip.*, vol. 711, pp. 21–26, 2013.

[39] J. Ely and B. Mcdonald, "Neutron and Gamma Ray Pulse Shape Discrimination with Polyvinyltoluene," March, 2012.

REPORT DOCUMENTATION PAGE

Form Approved
OMB No. 0704-0188

1. REPORT DATE *(DD-MM-YYYY)* 01-03-2018	2. REPORT TYPE Master's Thesis	3. DATES COVERED *(From - To)* September 2016 – March 2018

4. TITLE AND SUBTITLE	5a. CONTRACT NUMBER
Pulse Height Spectra Analysis of a Neutron Energy Tuning Assembly	5b. GRANT NUMBER
	5c. PROGRAM ELEMENT NUMBER

6. AUTHOR(S)	5d. PROJECT NUMBER
	5e. TASK NUMBER
Stickney, Jason R., Captain, USAF	5f. WORK UNIT NUMBER

7. PERFORMING ORGANIZATION NAME(S) AND ADDRESS(ES) Air Force Institute of Technology Graduate School of Engineering and Management (AFIT/EN) 2950 Hobson Way, Building 640	8. PERFORMING ORGANIZATION REPORT NUMBER AFIT-ENP-MS-18-M-098

9. SPONSORING / MONITORING AGENCY NAME(S) AND ADDRESS(ES) This block is intentionally left blank	10. SPONSOR/MONITOR'S ACRONYM(S)
	11. SPONSOR/MONITOR'S REPORT NUMBER(S)

12. DISTRIBUTION / AVAILABILITY STATEMENT
DISTRIBUTION STATEMENT A;
APPROVED FOR PUBLIC RELEASE; DISTRIBUTION UNLIMITED

13. SUPPLEMENTARY NOTES
This material is declared a work of the U.S. Government and is not subject to copyright protection in the United States.

14. ABSTRACT
An energy tuning assembly (ETA) was previously designed and built for the purpose of irradiating samples with a combination of a thermonuclear and a prompt fission neutron spectrum. Initial research was performed to characterize the performance of the ETA at the Lawrence Berkeley National Laboratory 88-Inch Cyclotron using 33 MeV deuteron breakup on tantalum as the neutron source. This research analyzes detector responses collected from three EJ-309 detectors used to characterize the ETA generated neutron field. A signal processing chain was developed to reduce the full waveform data into a pulse height spectrum. The primary goal was to develop a processing chain that optimized pulse shape discrimination performance to improve the discrimination between neutrons and gammas. It was found that the processing chain developed allowed for greater flexibility in determining the PSD parameters, which allowed for a greater degree of particle discrimination at low pulse heights.

15. SUBJECT TERMS
Pulse shape discrimination, neutron spectroscopy, energy tuning assembly, neutron detectors

16. SECURITY CLASSIFICATION OF:			17. LIMITATION OF ABSTRACT	18. NUMBER OF PAGES	19a. NAME OF RESPONSIBLE PERSON Capt James E. Bevins, AFIT/ENP
a. REPORT U	b. ABSTRACT U	c. THIS PAGE U	UU	79	19b. TELEPHONE NUMBER *(include area code)* (937)255-3636 x4767

Standard Form 298 (Rev. 8-98)
Prescribed by ANSI Std. Z39.18